MECHANISMS OF TRANSMEMBRANE SIGNALING BY BACTERIAL CHEMORECEPTORS: STUDIES OF DYNAMICS AND COFACTOR REACTIVITY

A Dissertation
Presented to the Faculty of the Graduate School
of Cornell University
in Partial Fulfillment of the Requirements for the Degree of
Doctor of Philosophy

by
Dipanjan Samanta
February 2016

Mechanisms of Transmembrane Signaling by Bacterial Chemoreceptors: Studies of Dynamics and Cofactor Reactivity

Dipanjan Samanta, Ph.D.

Cornell University 2016

Flagellated bacteria constantly and actively search for optimum niches for their survival and proliferation by swimming in the environment. A family of receptor proteins, named chemoreceptors or methyl-accepting chemotaxis proteins (MCPs), along with cellular energy sensor Aer and sensory rhodopsins (SR) guide the cells towards optimal chemical and spectral compositions by controlling the activity of intracellular kinase CheA and thereby regulating cellular taxes (or movements). These receptors also serve as model systems for transmembrane signal transduction and cell-environment interaction. Although the receiver domains in these receptors vary greatly in sequence, function, and even in disposition relative to the membrane, the cytoplasmic domains of all of these transmembrane proteins share high homology and signal through the same kinase CheA. We engineered two variants of the cytoplasmic domain of *E. coli* aspartate receptor Tar, H1-Tar and H1-2-Tar, that mimic the ligand unbound and bound states of the full length native receptor, respectively, in order to uncover the general principle behind kinase activity regulation. As translated, H1-Tar stimulates the kinase, whereas H1-2-Tar deactivates the kinase both in vivo and in vitro, despite similar binding to CheA. These variants also respond to the modifications in four conserved glutamate and glutamine residues as the native Tar: mutation of two glutamines to glutamates renders H1-Tar deactivating, whereas H1-2-Tar stimulates the kinase upon mutation of the two glutamates to glutamines. Continuous wave and pulsed dipolar electron spin resonance spectroscopic studies of the spin labeled variants reveal dynamical coupling throughout the cytoplasmic domain of MCPs and that dynamics in the two ends of the domain are inversely correlated. The dynamics in the membrane distal region of the domain, named protein interaction region (PIR) that interacts with the kinase via an adaptor protein CheW correlate with the activating state of the receptors: conformationally dynamic PIR deactivates CheA and relatively static

PIR activates the kinase. Thus, we find that these receptors regulate the kinase activity based on the receiver domain state and modifications in those conserved residues by altering the dynamics throughout the cytoplasmic domain. Of these receptor proteins, the state of the receptive PAS domain of the energy sensor Aer relevant for CheA activity modulation is not particularly well described. We have, for the first time, purified bacterial Aer and have confirmed that Aer PAS domain binds FAD as a cofactor. *In vitro* sodium dithionite treatment reversibly reduces FAD in Aer from fully oxidized state to the single electron reduced anionic semiquinone (ASQ) state supporting the notion that Aer FAD samples different redox states to modulate the kinase activity. We show that Aer in fully oxidized FAD state activates the kinase, whereas in ASQ state inhibits the kinase. These results suggest that Aer senses the electron flow in the electron transport chain through FAD bound at the PAS domain and modulates the kinase activity based on the FAD redox state. Overall, this dissertation gains insights into the mechanisms of how these transmembrane receptors regulate the kinase activity in order to govern bacterial motion in response to the environmental stimuli.

BIOGRAPHICAL SKETCH

Dipanjan Samanta was born in the family of Jaladhar Samanta and Supriya Samanta as the second child in the year of 1988 in Amarpur, a village in West Bengal state of India. His loving and caring parents and the elder brother, Nilanjan Samanta, provided him guidance throughout his life and encouraged him to study and learn various subjects since his young age as a means to open up and broaden the mental attitude. He went to the primary school, Amarpur Prathomik Vidyalaya, and later to the local high school, Gujarpur Surendranath Vidyapith, where he developed his interest in science and history. He pursued a Bachelor of Science (B.Sc.) degree in Chemistry at Ramakrishna Mission Vidyamandira, a college affiliated under University of Calcutta. After completing the degree in 2008, he continued higher studies at Indian Institute of Technology (IIT) at Kanpur and received Master of Science (M.Sc.) degree in Chemistry in 2010. During the summer of 2009, he was a Visiting Student Research Programme (VSRP) fellow at Tata Institute of Fundamental Research at Mumbai. Here in the lab of Professor Sudipta Maiti he investigated the effect of zinc ion and curcumin, the principal curcuminoid in turmeric, on amyloid beta aggregates, which are the crucial pathology of Alzheimer's disease, in order to understand the development of the disease and ideally to find a cure for the disease. During this period he developed fascination for molecular biology and biophysics research and learned various fluorescence techniques. During the M.Sc. project in 2010, he worked with Professor Debabrata Goswami at IIT Kanpur and learned various aspects and techniques in non-linear optics. Post M.Sc., he joined the Ph.D. program in the department of Chemistry and Chemical Biology at Cornell University, and investigated the mechanisms of the regulation of bacterial motion towards various environmental stimuli by transmembrane receptor proteins with Professor Brian R. Crane and Professor Jack H. Freed. Apart from science, he likes to sing and dance, and wishes to travel to major historical and cultural places throughout the world.

Dedicated to my parents, Jaladhar Samanta and Supriya Samanta, my elder brother Nilanjan Samanta, and my grandmothers, late Kananbala Samanta and Padmabati Guria

ACKNOWLEDGEMENTS

I am ever thankful to my advisors, Professor Brian R. Crane and Professor Jack H. Freed, for their invaluable suggestions, unstinting guidance and encouragements, and financial support. I am very much thankful to my committee members, Professor Richard A. Cerione and Professor John D. Helmann, for their support, encouragements and letting me use various instruments and facilities in their lab. I acknowledge here the numerous help and suggestions from the past and current members in Crane lab and Freed lab. I am thankful to Cornell University and the Department of Chemistry and Chemical Biology for the admission offer to the graduate program and the financial support.

I am so thankful to all my teachers, starting from primary school and high school to college and universities, for shaping my thoughts and outlook.

Tremendous love, support, and encouragements from my parents Jaladhar Samanta and Supriya Samanta, brother Nilanjan Samanta, grandmothers late Kananbala Samanta and Padmabati Guria, my friend Ananya Dutta, my extended family and many friends are invaluable in my life.

TABLE OF CONTENTS

Biographical Sketch ---------- (iii)
Dedication ---------- (iv)
Acknowledgements ---------- (v)
Table of Contents ---------- (vi)
List of Figures ---------- (ix)
List of Tables ---------- (xi)

Chapter One: Introduction

1.1 Bacterial Chemotaxis ---------- 1
1.2 Components of the *E. coli* Chemotaxis Signaling Pathway ---------- 3
1.2.1 MCP Receptors ---------- 3
1.2.2 The CheA Kinase and CheW Adaptor Protein ---------- 6
1.3 Signaling Mechanism of Bacterial Chemotaxis ---------- 7
1.4 Propagation of ligand-binding signal to the kinases ---------- 9
1.5 Distance measurements in biomolecules with double electron electron resonance technique ---------- 11
1.6 References ---------- 16

Chapter Two: Bacterial Chemoreceptor Dynamics Correlate with Activity State and Are Coupled over Long Distances

2.1 Introduction ---------- 29
2.2 Results
2.2.1 CheA activity and ternary complex stability ---------- 33
2.2.2 Conformational differences in the KCM ---------- 34
2.2.3 Effector modification inverts conformational dynamics ---------- 39
2.2.4 Dynamic measurements by CW-ESR ---------- 43
2.3 Discussion ---------- 47

2.4 Materials and Methods
2.4.1 Cloning, Expression and Purification of Proteins ---------- 51
2.4.2 *In vivo* activity of H1-Tar and H1-2-Tar ---------- 52
2.4.3 *In vitro* CheY phospho-transfer assay ---------- 52
2.4.4 Pull-down Experiments ---------- 52
2.4.5 Site Directed Spin Labeling ---------- 53
2.4.6 Pulsed Dipolar ESR Measurement ---------- 54
2.4.7 CW ESR Data Collection and Analysis ---------- 54
2.5 Acknowledgements ---------- 55
2.6 References ---------- 56

Chapter Three: Bacterial Energy Sensor Aer Modulates Activity of the Chemotaxis Kinase CheA Based on Redox State of Flavin Adenine Dinucleotide Cofactor

3.1 Introduction ---------- 62
3.2 Results ---------- 64
3.3 Discussion ---------- 68
3.4 Methods
3.4.1 *E. coli* Aer Expression and Purification ---------- 69
3.4.2 Aer incorporation into nanodisc ---------- 70
3.4.3 Sodium dithionite reduction of Aer and aerial reoxidation ---------- 70
3.4.4 cw-ESR spectra collection ---------- 70
3.4.5 CheY phosphotransfer assay ---------- 71
3.5 References ---------- 72

Chapter Four: Means for the Propagation of Allosteric Communications

4.1 Introduction ---------- 76
4.2 Allosteric transmission involving mainly conformational changes in the intervening regions ---------- 78

4.3 Allosteric transmission mainly involving dynamical changes in the intervening regions ---------- 80
4.4 References ---------- 83

Appendix A: A Plausible Model Describing Modulation of Bacterial Chemotaxis Kinase Activity by Chemoreceptors Dynamics Alteration ---------- 90

Appendix B: Redox State of Flavin Adenine Dinucleotide Cofactor Determines Aer Mediated Bacterial Phototaxis in Response to Blue Light ---------- 92

LIST OF FIGURES

Figure 1-1 Bacterial chemotaxis ---------- 1
Figure 1-2 Structures of different segments of MCPs ---------- 5
Figure 1-3 Structural details of the CheA domains and CheW ---------- 7
Figure 1-4 Schematic of the signaling pathway in bacterial chemotaxis -------- 8
Figure 1-5: Spin labeling a protein ---------- 12
Figure 1-6: Spin interaction and pulse sequence for 3-pulse DEER ---------- 12
Figure 1-7: A pictorial description of the DEER mechanism ---------- 13
Figure 1-8: Pulse sequence of 4-pulse DEER ---------- 14
Figure 2-1 Schematic representations of spin-separations generated by different helix packing and labeling locations ---------- 32
Figure 2-2 Properties of the H1-Tar and H1-2-Tar effectors ---------- 33
Figure 2-3 Dynamical properties of the HAMP-KCM inferred by PDS ---------- 36
Figure 2-4 Constancy of signaling properties of mutated and spin labeled effectors ---------- 38
Figure 2-5 Modification of adaptation sites reveals allosteric coupling throughout the HAMP-KCM ---------- 40
Figure 2-6 Typical SDS-PAGE analysis of DEER/CW ESR samples ---------- 41
Figure 2-7 CW–ESR spectra reflect dynamic differences in HAMP and KCM - 44
Figure 2-8 Deconvolution of the CW ESR spectra into two components -------- 44
Figure 2-9 Variation of CW ESR spectra with temperature ---------- 46
Figure 2-10 Dynamical properties of the HAMP-KCM ---------- 50
Figure 3-1 A hypothesis that connects FAD redox states with different modes of cellular movement ---------- 63
Figure 3-2 Purification and chemical reduction of EcAer ---------- 64
Figure 3-3 Quantification of FAD binding to Aer and the effect of detergent on CheA activity ---------- 65
Figure 3-4 Characterization and functional implication of various redox states of FAD in Aer ---------- 67

Figure 3-5 Control experiment showing no interference of dithionite on CheA activity ---------- 67
Figure 4-1 Different states of the motifs/domains intervening the allosterically coupled sites can be characterized by differences in structure and/or dynamics ---------- 77
Figure Appendix A-1 A model that links dynamics in chemoreceptors with the kinase activity ---------- 91
Figure Appendix B-1: Blue light reduction of FAD cofactor in EcAer ---------- 92

LIST OF TABLES

Table 2-1 Parameters of the distance distribution for each site at QEQE adaptation state ---------- 37
Table 2-2 Comparison of the parameters of distance distributions at different adaptational states ---------- 42
Table 2-3 Quantification of the slow and fast component from CW-ESR spectra ---------- 46
Table 2-4 Motional parameters for the mobile components ---------- 47

Chapter One

Introduction

1.1 Bacterial Chemotaxis:

Bacterial chemotaxis (1–3) is a process that guides flagellated bacteria towards the optimal chemical environment as demanded by its metabolic requirements. The process is best explored in *Escherichia coli*; hence here onwards *E. coli* chemotaxis is described in detail. In isotropic media, multi-flagellated *E. coli* move with two distinct phases: relatively long "runs" that last up to several seconds (i.e. swimming in almost a straight line) and brief "tumbling" for ~0.1 s that interrupts the run. Bacteria "run" when flagella rotate in counter-clockwise (CCW) direction producing a flagellar bundle that propels the cells forward, whereas stochastic reversal of flagellar rotation to the clockwise (CW) direction causes cellular tumbling that reorients the cell for the next "run". In anisotropic media with concentration gradient of chemicals *E. coli* search out the optimal chemical niches by regulating the duration of the "run" and "tumbling". When the cells steer up the concentration gradient of beneficial chemicals (attractants) or steer down the gradient of harmful chemicals (repellents), the chemotactic process lengthens the "runs" by biasing the flagellar rotation in the counter-clockwise (CCW) direction. In contrast, cells tumble more upon encountering decreasing concentration of attractants and/or increasing repellent concentration by inducing clockwise (CW) rotation of the flagella, which leads to the disassembly of flagellar bundle. As each flagellum separated from the others propels the cell in a unique direction, the cell reorients (Fig. 1-1) (4, 5).

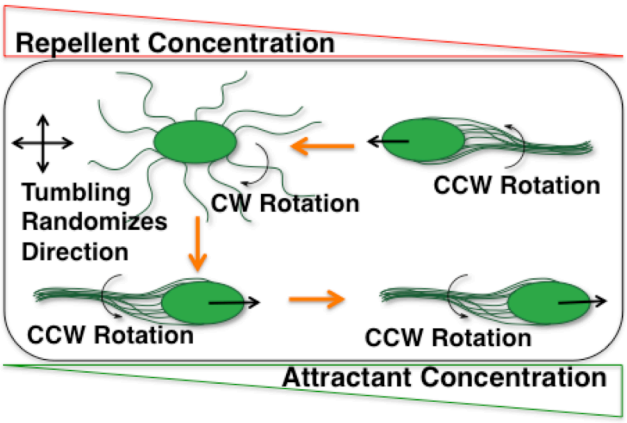

Figure 1-1: *E. coli* chemotaxis: An *E. coli* cell is depicted at different stages during Chemotaxis.

The chemotaxis system detects chemicals in the environment, transmits the information to the interior of the cell and processes the information to enable the cell to alter its behavior; for its relative simplicity, chemotaxis serves as a model system for transmembrane signaling. The system displays exceptionally high sensitivity, gain, and cooperativity, wide sensing range, and precise adaptation (6–8). Bacterial chemotaxis senses a wide range of ligand concentrations from 300 nM to 100 mM for α-methyl aspartate spanning six orders of magnitude (9). The sensing range varies with the specific ligand under consideration. At the same time, the system can detect a change of only 1% in the ligand occupancy (10, 11), which elicits up to 50% change in the rotational bias of the flagella (10) and up to 36 fold change in the activity of the intracellular proteins (12). This high gain in the process indicates that the underlying signaling pathway is highly cooperative and, as a matter of fact, Hill coefficients as high as 10 have been observed for the stimulus-response curve (13, 14). With these exceptional features bacterial chemotaxis pathway has provided a basis for numerous experimental, theoretical (15, 16), and evolutionary (17) studies over the past several decades. The chemotaxis system is also similar to and shares components with other microbial taxis systems, namely phototaxis (18, 19), which steers cells based on the quality and quantity of light, and energy taxis (20–22) that directs bacteria towards optimum energy producing environment.

Chemotaxis has also been associated with several microbial diseases such as cholera by *Vibrio cholerae* (23, 24), gastritis and duodenal ulcer by *Helicobacter pylori* (25, 26), Lyme disease by spirochete (27), and salmonellosis by *Salmonella* (28), for directing the pathogens to their niches inside the host's body, and thereby assisting in the diseases. The unique ability of the chemotaxis system to guide bacteria toward a source offers a potential means to appropriate the system for various applications including the identification and killing of

cancer cells (29, 30). Thus, health concerns also spur research on bacterial chemotaxis.

1.2 Components of the *E. coli* Chemotaxis Signaling Pathway:

The chemotaxis pathway involves two transmembrane protein complexes: a receptor signaling complex and a flagellar assembly, which together sense the chemical environment and elicit the required changes in the movement of bacteria. The receptor signaling complex includes the receptor proteins, named methyl-accepting chemotaxis protein (MCP) (31), intracellular kinase CheA (32–34), and the cytoplasmic adaptor protein CheW (35–37) that couples CheA to MCPs. The flagellar assembly is a highly complex structure and resembles a macroscopic motor (6, 38). It consists of more than 50 gene products and controls the direction of flagella rotation based on the information input from the signaling complex. In addition to the two membrane complexes, the core signaling pathway also comprises several cytoplasmic proteins: the response regulator CheY (39–41), which transmits the signal from the signaling complex to the flagella, the phosphatase CheZ (42), which terminates the excitation signal by dephosphorylating CheY, and the receptor modification enzymes: the methyl-transferase CheR (43–45), and methylase CheB (46, 47). The kinase CheA and the response regulator CheY characterize the chemotaxis pathway as the two-component signaling mechanism, widespread in bacteria and archaea (48–51).

1.2.1 MCP Receptors:

Receptors in the *E. coli* MCP family vary in the abundance: high-abundant Tsr and Tar sense and respond to the attractant serine, and aspartate and maltose, respectively, whereas low abundant Trg and Tap mediate taxis respectively towards ribose and galactose, and dipeptide (52, 53). Tar also responds to the repellent Ni^{+2} ion (54). Another receptor Aer, which monitors internal energy of the cell and thereby directs it towards optimum energy generating environment (55, 56), is similar to the other chemoreceptors and normally is included into the MCP family.

MCPs are homodimeric transmembrane receptor proteins that assemble into the functional unit of a trimer-of-dimers (14, 57–59), which comprises either like or mixed receptors as a means to integrate information about different chemicals in the environment (60–63). These trimers-of-receptor dimers organize into extended hexagonal arrays mostly in the cell poles (64–66) and engage CheW and CheA in the cytoplasm in order to regulate the kinase activity effectively and cooperatively (36, 67–70). Each homodimer contains a periplasmic domain, a transmembrane region, and in the cytoplasm, a membrane proximal HAMP domain and a kinase control module (KCM) (Fig. 1-2). From HAMP proximal to the distal end, the KCM is subdivided into adaptation, glycine hinge, and protein interaction regions (17). Each subdomain is functionally unique. The periplasmic domain binds ligands in the periplasm (71, 72). The transmembrane region transmits the conformational changes in the periplasmic domain upon ligand binding across the lipid bilayer. The HAMP domain, widely found in **H**istidine kinases, **A**denylyl cyclases, **M**ethyl-accepting chemotaxis proteins, and **P**hosphatases, is a signal conversion module that relays the input signal from the transmembrane region to the KCM to modulate the activity of the kinase CheA (73–75). The adaptation region contains four or five specific glutamates and glutamine residues that undergo reversible methylation by CheR and CheB, which together equip the chemotaxis process with the ability to adapt to the level of stimulus (76). The glycine hinge region allows deformation in the receptor structure in order to facilitate higher order arrangements (77) that in turn, favors the high cooperativity of the process. The protein interaction region directly binds to and regulates the activity of CheA, and also provides the interaction surfaces to form the trimer-of-dimers.

MCPs have a ~380 Å long helical structure that spans periplasm, lipid bilayer, and cytoplasm (Fig. 1-2A). Each subunit contributes four helices, α1 through α4, to the periplasmic domain (Fig. 1-2B), among which α4 is contiguous with transmembrane helix 2 (TM2) (72, 78). The transmembrane region is constituted from four helices (TM1/TM1’ and TM2/TM2’), two of which are donated by each subunit. TM1 extends into the periplasm to construct the α1 helix. The HAMP

domain is a parallel four-helical coiled coil structure (73, 74) with two helices (AS1/AS2 or AS1'/AS2') provided by individual subunits (Fig. 1-2C). Directly attached to the HAMP domain is a long extended antiparallel dimeric four-helix bundle (helices CD1/CD2 or CD1'/CD2') that forms the KCM (Fig. 1-2D) (58, 79). The C-terminal residues of the KCM form an NWETF motif that binds the adaptation enzymes CheR and CheB to facilitate modifications of the adaptation region (Fig. 1-2A) (80, 81).

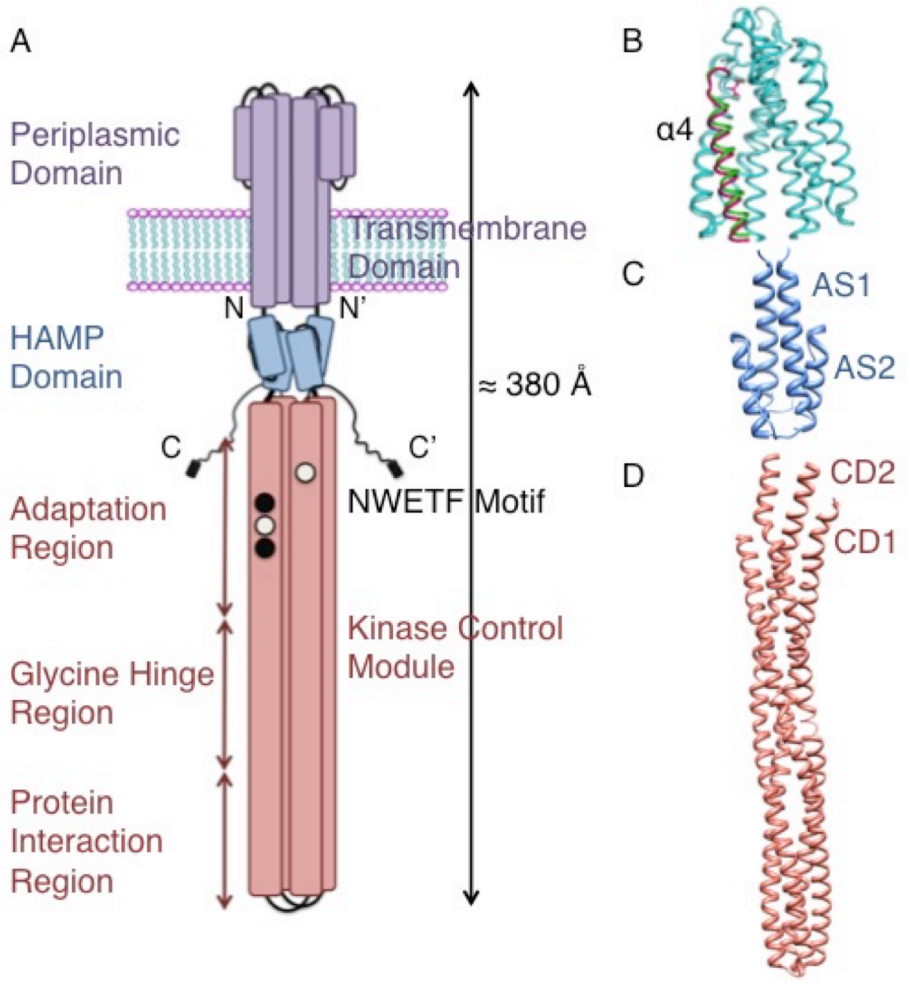

Figure 1-2: Structures of different segments of MCPs: (A) Schematic of a transmembrane MCP displays the relative disposition of all of the subdomains relative to the lipid bilayer. Black and white circles, respectively, represent the specific glutamate and glutamine residues in the adaptation region. The black cylinders at the end of the C termini represent the NWETF motifs. (B) Structures

of the periplasmic domain in apo- and aspartate-bound state of E. coli Tar (PDB IDs: 1LIH and 1WAT, respectively) are superimposed to depict the conformation change in the α4 helix that occurs upon ligand binding (green = apo state and red = ligand bound state, respectively) that apart from which the two structures overlap very well. The aspartate is shown in red stick. (C) The structure of HAMP1 from the P. aeruginosa HAMP1-2-3 (PDB ID: 3LNR) (D) The antiparallel four helical structure of the KCM in E. coli Tsr is adapted from PDB ID: 1QU7.

1.2.2 The CheA Kinase and CheW Adaptor Protein:

The histidine kinase CheA is a homodimeric multidomain protein containing five domains, P1 through P5. The four helical P1 domain contains the conserved histidine (H48 in *E. coli* and H45 in *T. maritima*) that undergoes phosphorylation to transfer the phosphoryl group to the conserved aspartate residues of the response regulators CheY and CheB (Fig. 1-3A, B) (34, 82). The least conserved P2 domain has α/β structure and facilitates phosphotransfer by binding the response regulators and thereby increasing their proximity to the P1 domain (Fig. 1-3B) (33, 83). The P3 is dimerization domain and assumes an antiparallel four-helix bundle structure similar to that of the receptors. The catalytic P4 domain binds adenosine triphosphate (ATP) and phosphorylates the histidine in the P1 domain, whereas the regulatory P5 domain binds the protein interaction region in the receptor and CheW to exert the receptor influence on the kinase activity (Fig. 1-3C) (32). The P2 domain is attached to P1 and the core of the kinase formed by P3-P4-P5 domains via two linkers, which allows flexibility to the P1 and P2 domains for proper functional regulation.

The structural complementarity of the CheW and the P5 domain permits the interaction of the two, which in turn facilitates the higher order hexagonally packed arrangement of the trimers of receptor dimers linked by networks of the kinase and the adaptor protein (Fig. 1-3D) (84).

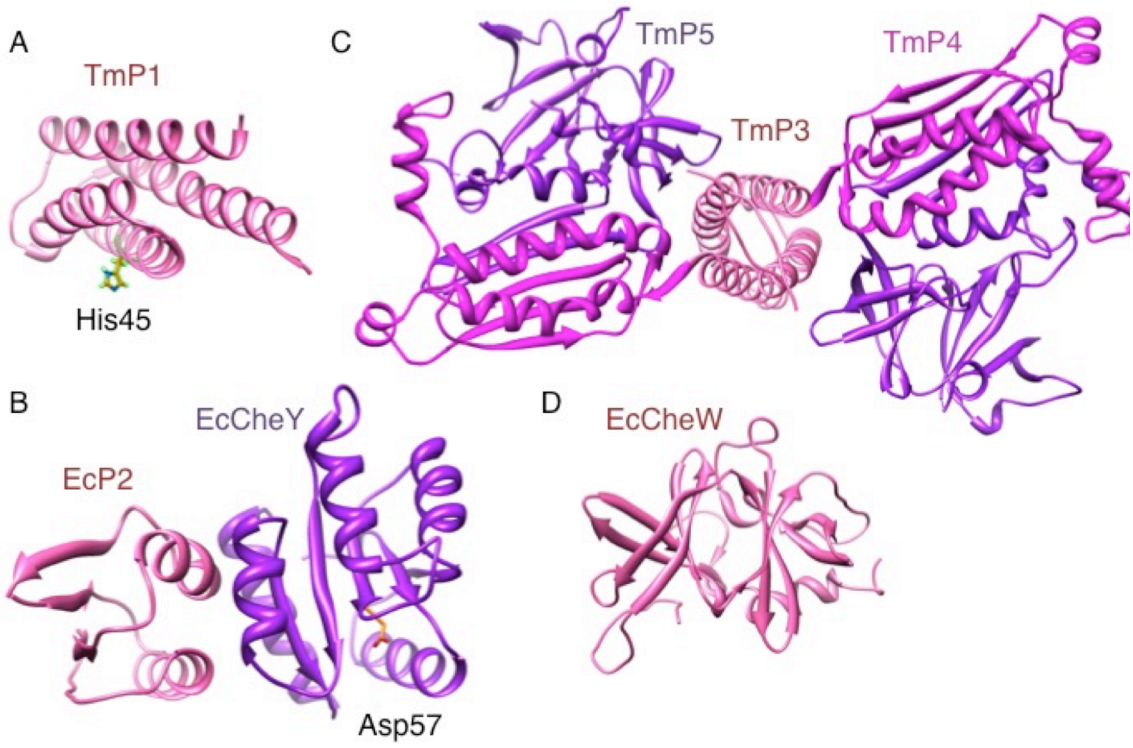

Figure 1-3: Structural details of the CheA domains and CheW: (A) First four helices of the P1 domain are depicted from *T. maritima* (PDB ID: 1TQG) with the conserved histidine. (B) Based on PDB ID: 1EAY, the complex of P2 domain and CheY, both from *E. coli*, is represented with the conserved aspartate residue. (C) The core structure of CheA dimer, formed by P3, P4, and P5 domains, is adapted from PDB ID: 1B3Q. (D) The three dimensional structure of *E. coli* CheW is delineated (PDB ID: 2HO9).

1.3 Signaling Mechanism of Bacterial Chemotaxis:

Multiple proteins coordinate their functions to propagate chemoattractant signals from the outside of the cell to the flagellar motor (6, 85, 86) (Fig. 1-4). Bacterial chemoreceptors or MCPs detect and bind specific chemicals in the periplasmic domain as the first step of the signaling mechanism. Repellent binding transduces an activating signal through the receptors to the kinases in order to catalyze auto-phosphorylation of CheA, the step where the ATP bound in the P4 domain phosphorylates His48 in the P1 domain. The phosphate group from the P1 domain is transferred to Asp57 in the CheY bound to the P2 domain. The

phosphorylated CheY (CheY-P) diffuses in the cytoplasm and binds to the motor protein FliM in the flagella complex causing CW rotational bias of the flagella, which leads to cellular tumbling and eventually a change in the swimming direction. Attractant binding, on the other hand, deactivates the kinase leading to discontinuation of CheY phosphorylation. CheY-P auto-dephosphorylates on the time scale of 10 s, but the phosphatase CheZ accelerates dephosphorylation 100 fold (0.1 s) (87). CheZ co-localizes with the signaling complex via an allele of CheA, $CheA_S$, that lacks the first four helices in the P1 domain (88). Lower binding affinity of dephosphorylated CheY for FliM induces its dissociation from the flagellar assembly and thereby, promotes CCW rotational bias of the flagella. Thus, by modulating kinase activity, chemoreceptors govern the chemotaxis process.

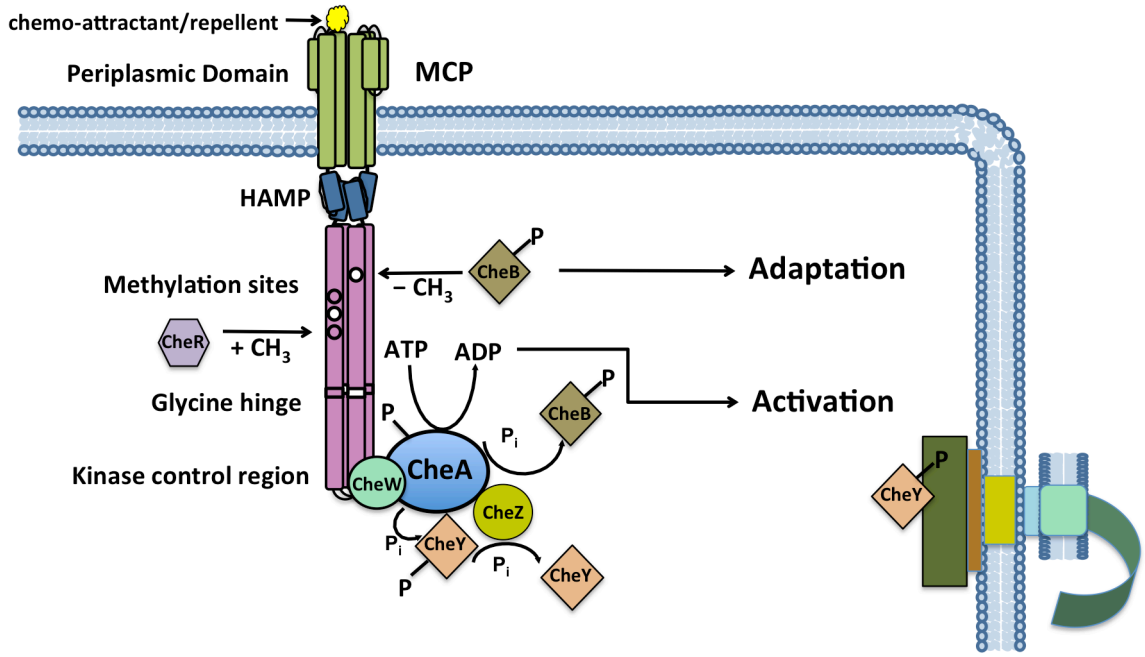

Figure 1-4: Schematic of the signaling pathway in bacterial chemotaxis.

The bacterial chemotaxis system has the ability to precisely adapt to a new environment and to retain sensitive detection over a wide range of chemical concentration. The adaptation enzymes CheR and CheB together endow the system with these qualities by providing feedback of current conditions to the

system. The response regulator CheB is phosphorylated and thus activated by the kinase CheA, whereas the methyltransferase CheR is constitutively active. Activated CheB demethylates or deamidates, respectively, the methylated form of the specific glutamates and the specific glutamines on the receptors (Fig. 1-2A) (89, 90), and counteracts the activating effect of repellent binding by transmitting a deactivating signal to the kinase. On the other hand, CheR methylates the glutamates encoded by the gene or generated after deamidation of the glutamines as a means to activate the kinase and oppose the effect of attractant binding (91, 92). Thus, along with chemical binding in the periplasmic domain, the methylation state of the adaptation region on the receptor dictates the kinase activity (14). This negative feedback loop in turn restores CheA activity to the pre-stimulus level and as a result cells adapt to a new environment. Mutation of the glutamate residues to glutamine residues *in vitro* has been shown to functionally mimic the consequence of methylation of the receptors. Different methylation levels translate the cooperative ligand-response curve of the signaling complex along the axis of ligand concentration by altering the dissociation constant of periplasmic domain for the ligand (93–95). Thus, the CheR-CheB pair assists the chemotaxis process to retain wide sensing range by maintaining sensitive detection in very different ligand concentrations.

1.4 Propagation of ligand-binding signal to the kinases:

Cell surface receptor proteins, such as G-protein-coupled receptors and receptor tyrosine kinases, enable cells to interact with and thereby adapt to the changes in the surroundings by binding the ligands in the extracellular regions and transducing the ligand binding signal to the interior of the cell (96–98). Thematically MCPs are similar to the other cell surface receptor proteins as they also regulate an intracellular phosphorylation cascade based on the chemicals detected in the periplasmic space, yet they are notable because of the distance over which allostery propagates: CheA binds to the protein interaction region, almost 380 Å away from the ligand binding pocket. So, a comprehensive knowledge of how the allostery is transmitted through the chemoreceptors over such a long distance to modulate the activity of the kinase is valuable, as that

would potentially reveal general mechanisms of how conformational changes are relayed in large modular proteins. A piston-like displacement of the α4 helix and the transmembrane helix 2 (TM2) towards the cytoplasm upon attractant binding has been shown by crystallography, electron spin resonance (ESR) spectroscopy, solid state nuclear magnetic resonance (ssNMR) spectroscopy and other biophysical methods (78, 99, 100). But, how this conformational change is propagated in the cytoplasmic domain of the receptors is a contentious topic.

Three models have been proposed for the HAMP mechanism, with each supported by some lines of experimental evidence. (A) After comparison of the crystal structure of an archeal HAMP domain with the canonical “knob into hole” structure of four helix bundle, a gear-box model has been presented as the HAMP mechanism in which the helices rotate with respect to each other to switch between the proposed two states: “knob into hole” and “knob to knob” structures (73). (B) Cysteine and disulfide scanning studies suggest a scissor like motion of the HAMP helices as the mechanism of sending the piston displacement in the TM2 to the KCM (101). (C) A large dataset of mutational analyses generates a biphasic stability model in which moderately stable HAMP domain transmits activating signal to the kinase, whereas both of highly stable and unstable HAMP domains deactivate CheA (102, 103). Various other methods including pulse-dipolar ESR spectroscopy support this model (104).

Unlike disparate models for HAMP action, the KCM has been widely accepted as a dynamic structure that alters its dynamical properties as a means to propagate the ligand-binding signal to the kinase (62, 101, 105, 106). In spite of this general acceptance, the detail of the changes in dynamics is highly debated (101, 105, 106). Apart from that, a rotational model also exists for signal transmission through the KCM (107). A considerable part of this dissertation is devoted towards allosteric propagation in the cytoplasmic domain of the chemoreceptors. The dynamics alteration in KCM has been implicated to regulate the sequestration and mobility of P1 and P2 domains of the kinase as a means to

modulate autophosphorylation rate of CheA, although the details of this is to be further explored (108, 109).

1.5 Distance Measurements in Biomolecules with Double Electron Electron Resonance (DEER) Technique:

Functions of biomolecules are often encoded by their three-dimensional (3D) structure, which can be defined either by the relative coordinates of all the atoms or by the pairwise distances between the atoms in the molecule. X-ray crystallography and cryo-electron microscopy solves for the former criteria to determine the structure, whereas small angle X-ray scattering (SAXS), fluorescence resonance energy transfer (FRET), measurement of nuclear overhauser effect (NOE) in nuclear magnetic resonance (NMR), and various techniques in electron spin resonance (ESR) seek for the latter constraints. This chapter elaborates on a particular distance measurement technique of ESR called double electron electron resonance (DEER).

Being an ESR technique, DEER is sensitive to magnetic moments arising from unpaired electron spins. However, biomolecules are diamagnetic in nature, necessitating labeling them with spin labels site specifically. Spin labels are stable chemical compounds containing unpaired electrons, and relevant functional groups for modifying biomolecules at a precise location (110, 111). For proteins, common practice is to generate a cysteine-less variant that preserves the function of the native protein and then to introduce a cysteine site specifically by mutating the corresponding gene with polymerase chain reaction (PCR) followed by covalent modification of the cysteine with a cysteine-specific spin label, MTSL (Fig. 1-5). To measure distance with DEER, at least two protein sites must be modified with the spin label.

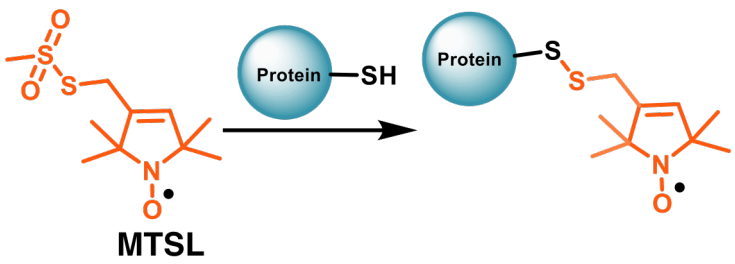

Figure 1-5: Spin labeling a protein. Protein molecule is depicted as a cyan sphere and the SH group refer to the cysteine residue at the surface of the protein that reacts with the MTSL to be spin labeled. Two such labels are required for DEER.

DEER is a spin echo-based pulse ESR technique that probes the dipolar interaction between the two spins selectively and very accurately (112, 113). The dipolar coupling ω_{ee} (r, θ) is defined as:

$$\omega_{ee}(r,\theta) = \omega_d[1 - 3\cos^2(\theta)]$$

with

$$\omega_d = \gamma_e^2 \hbar^2 / r^3$$

for two like spins, such as two MTSL labels. In these equations, r is the distance between the two spin centers, θ is the angle between **r** vector and the direction of applied magnetic field (Fig. 1-6A), and γ_e is the gyromagnetic ratio for the spins.

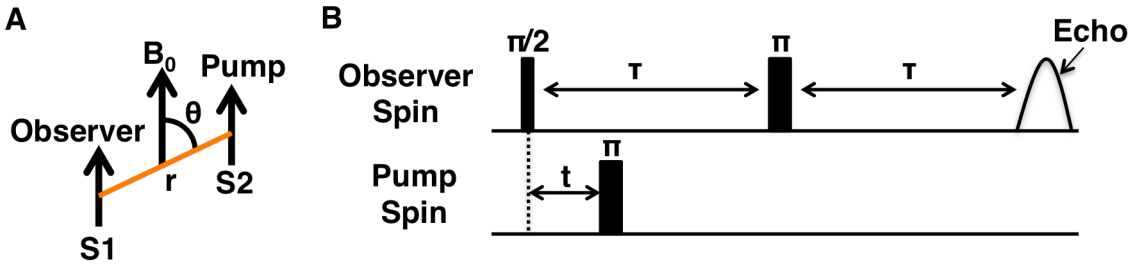

Figure 1-6: Spin interaction and pulse sequence for 3-pulse DEER. (A) A schematic shows the distance vector **r** between two spins, spin 1 (S1) or observer spin and spin 2 (S2) or pump spin, and the magnetic field meet at angle θ. (B) Pulse sequence of 3-pulse DEER is depicted with τ being fixed and t being variable.

Pulse sequence of 3-pulse DEER (114), one of the variations of the technique, is depicted in Fig. 1-6B. The sequence is comprised of a spin echo at resonance frequency of a selective set of total spins, called the observer spins (S1), and another π pulse at a separate frequency at which another set of total spins, called pump spins (S2), resonate. The pump π pulse is applied at variable times

after the first π/2 pulse. DEER monitors modulation of the echo signal arising from the observer spins due to π pulse-induced population inversion of the pump spins that couples the observer spins with dipolar interaction. Being an echo technique, DEER effectively removes electronic and nuclear Zeeman interactions, hyperfine interaction, and also electron electron dipolar interaction within observer spins set. Vector diagrams in Fig. 1-7 depict the states of the magnetizations at various moments during the experiment.

Observer Spin Magnetization without Pump π Pulse:

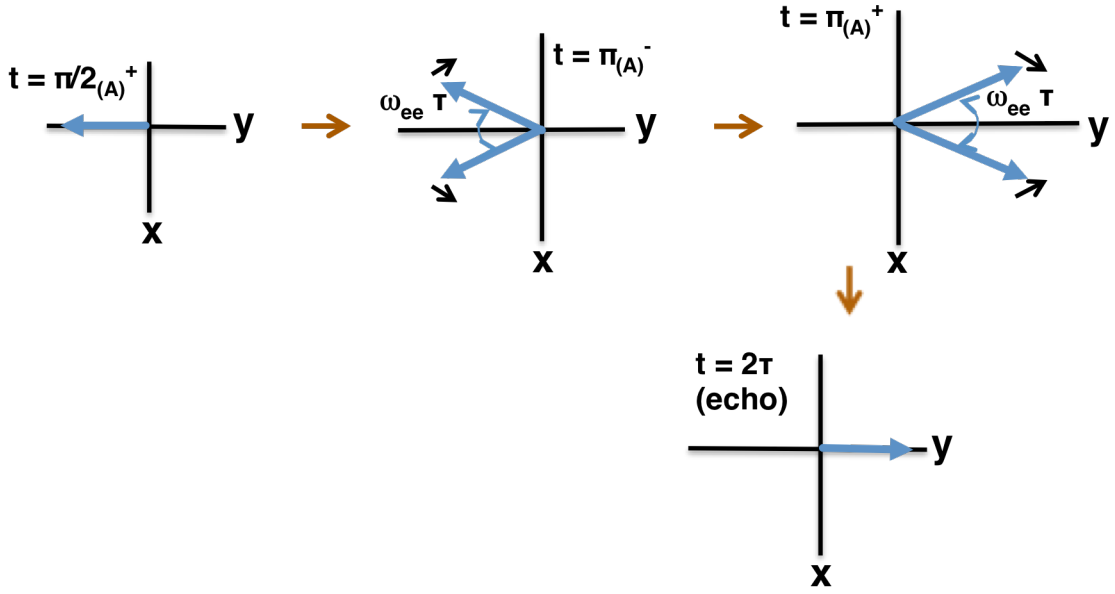

Observer Spin Magnetization with Pump π Pulse:

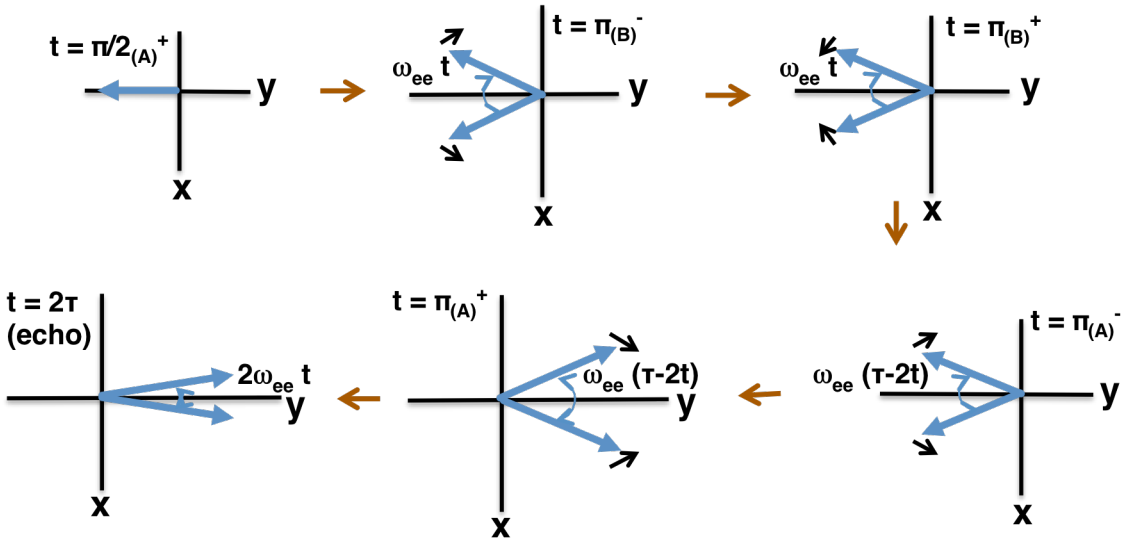

Figure 1-7: A pictorial description of the DEER mechanism. Vector diagrams illustrate the magnetization arising from the observer spins at various moments during the pulse sequence with and without the pump π pulse.

The first π/2 pulse tips the net magnetization from the observer spins in the x-y plane. Different energy of the two halves of the observer spins due to interaction with either of the two states of the pump spins (ms = + ½ or ms = - ½) causes the two halves of the magnetization to diverge in the rotating frame of reference. These two halves of the magnetization will coalesce if the pump π pulse is not provided. However, as the pump π pulse inverses the population of the pump spins, energy of the two halves of the observer spins is altered upon application of the pump π pulse. As a consequence the echo signal intensity is modulated as a function of cos (ω_{ee} t). From the modulation frequency distance or distance distribution between the two spin labels is calculated using Tikhonov regularization method (115) followed by a refinement using maximum entropy method (116).

As the microwave pulses applied are not exactly rectangular in time, they impose an issue of dead time, during which application of another pulse creates unwanted aberrations. This issue limits collection of early time data points, during which signal from a broad distance distribution disappears. Another variation, called 4-pulse DEER, smoothly avoids the dead time issue by introducing double echo sequence (Fig. 1-8) (117).

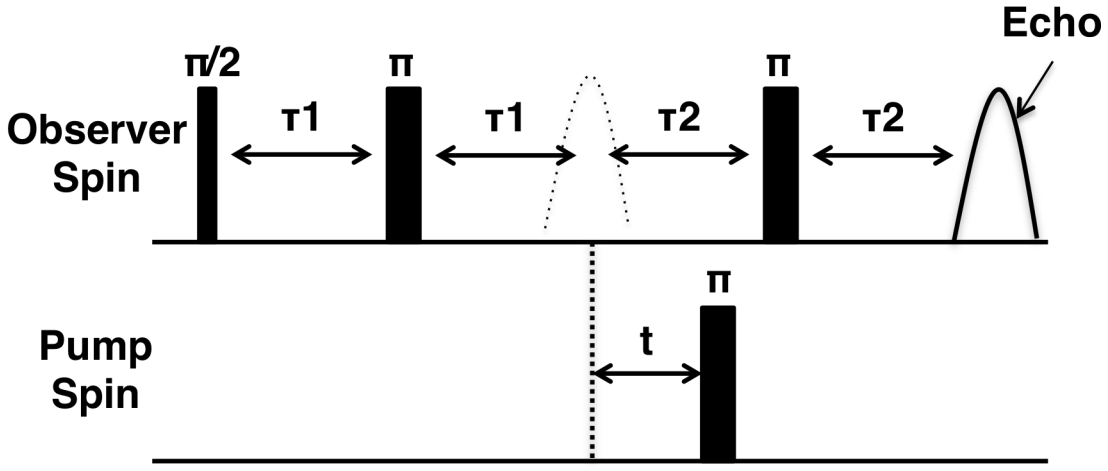

Figure 1-8: Pulse sequence of 4-pulse DEER. 4-pulse DEER sequence is depicted with τ1 and τ2 being fixed intervals for the two spin echos and t being variable time. The virtual echo signal is shown as a dotted envelope.

Distance distributions between two fixed sites in a protein or protein complex encode structure in the maximum probable distance and local dynamics in the breadth of the distribution (106). All the distance distribution data shown in this dissertation have been collected from flash cooled frozen samples with 4-pulse DEER operated at 17.35 GHz.

1.6 References:

1. Adler J (1966) Chemotaxis in Bacteria. *Science* 153(3737):708–716.

2. Tso W-W, Adler J (1974) Negative Chemotaxis in Escherichia coli. *J Bacteriol* 118(2):560–576.

3. Adler J (1975) Chemotaxis in Bacteria. *Annu Rev Biochem* 44(1):341–356.

4. Vladimirov N, Sourjik V (2009) Chemotaxis: how bacteria use memory. *Biol Chem* 390(11):1097–1104.

5. Sourjik V, Wingreen NS (2012) Responding to chemical gradients: bacterial chemotaxis. *Cell Regul* 24(2):262–268.

6. Wadhams GH, Armitage JP (2004) Making sense of it all: bacterial chemotaxis. *Nat Rev Mol Cell Biol* 5(12):1024–1037.

7. Parkinson JS, Ames P, Studdert CA (2005) Collaborative signaling by bacterial chemoreceptors. *Cell Regul* 8(2):116–121.

8. Hazelbauer GL, Falke JJ, Parkinson JS (2008) Bacterial chemoreceptors: high-performance signaling in networked arrays. *Trends Biochem Sci* 33(1):9–19.

9. Mesibov R, Ordal GW, Adler J (1973) The Range of Attractant Concentrations for Bacterial Chemotaxis and the Threshold and Size of Response over This Range: Weber law and related phenomena. *J Gen Physiol* 62(2):203–223.

10. Segall JE, Block SM, Berg HC (1986) Temporal comparisons in bacterial chemotaxis. *Proc Natl Acad Sci U S A* 83(23):8987–8991.

11. Jasuja R, Yu-Lin, Trentham DR, Khan S (1999) Response tuning in bacterial chemotaxis. *Proc Natl Acad Sci* 96(20):11346–11351.

12. Sourjik V, Berg HC (2002) Receptor sensitivity in bacterial chemotaxis. *Proc Natl Acad Sci* 99(1):123–127.

13. Li G, Weis RM (2000) Covalent Modification Regulates Ligand Binding to Receptor Complexes in the Chemosensory System of Escherichia coli. *Cell* 100(3):357–365.

14. Sourjik V, Berg HC (2004) Functional interactions between receptors in bacterial chemotaxis. *Nature* 428(6981):437–441.

15. Tindall MJ, Porter SL, Maini PK, Gaglia G, Armitage JP (2008) Overview of mathematical approaches used to model bacterial chemotaxis I: the single cell. *Bull Math Biol* 70(6):1525–1569.

16. Tindall MJ, Gaffney EA, Maini PK, Armitage JP (2012) Theoretical insights into bacterial chemotaxis. *Wiley Interdiscip Rev Syst Biol Med* 4(3):247–259.

17. Alexander RP, Zhulin IB (2007) Evolutionary genomics reveals conserved structural determinants of signaling and adaptation in microbial chemoreceptors. *Proc Natl Acad Sci* 104(8):2885–2890.

18. Suzuki D, Irieda H, Homma M, Kawagishi I, Sudo Y (2010) Phototactic and chemotactic signal transduction by transmembrane receptors and transducers in microorganisms. *Sensors* 10(4):4010–4039.

19. Klare JP, Bordignon E, Engelhard M, Steinhoff H-J (2011) Transmembrane signal transduction in archaeal phototaxis: the sensory rhodopsin. *Eur J Cell Biol* 90(9):731–739.

20. Taylor BL (1983) How do bacteria find the optimal concentration of oxygen? *Trends Biochem Sci* 8(12):438–441.

21. Zhulin I, Johnson M, Taylor B (1997) How Do Bacteria Avoid High Oxygen Concentrations? *Biosci Rep* 17(3):335–342.

22. Taylor BL, Zhulin IB, Johnson MS (1999) Aerotaxis and other energy-sensing behavior in bacteria. *Annu Rev Microbiol* 53:103–128.

23. Butler SM, Camilli A (2004) Both chemotaxis and net motility greatly influence the infectivity of Vibrio cholerae. *Proc Natl Acad Sci U S A* 101(14):5018–5023.

24. Butler SM, Camilli A (2005) Going against the grain: chemotaxis and infection in Vibrio cholerae. *Nat Rev Micro* 3(8):611–620.

25. Worku ML, Karim QN, Spencer J, Sidebotham RL (2004) Chemotactic response of Helicobacter pylori to human plasma and bile. *J Med Microbiol* 53(Pt 8):807–811.

26. Terry K, Williams SM, Connolly L, Ottemann KM (2005) Chemotaxis Plays Multiple Roles during Helicobacter pylori Animal Infection. *Infect Immun* 73(2):803–811.

27. Lux R, Moter A, Shi W (2000) Chemotaxis in pathogenic spirochetes: directed movement toward targeting tissues? *J Mol Microbiol Biotechnol* 2(4):355–364.

28. Stecher B, et al. (2004) Flagella and Chemotaxis Are Required for Efficient Induction of Salmonella enterica Serovar Typhimurium Colitis in Streptomycin-Pretreated Mice. *Infect Immun* 72(7):4138–4150.

29. Eils R, et al. (2010) Use of bacteria for the sensing and killing of cancer cells. Available at: http://www.google.com/patents/WO2010049375A1?cl=en.

30. Kumar AS, Bryan JN, Kumar SR (2014) Bacterial Quorum Sensing Molecule N-3-Oxo-Dodecanoyl-L-Homoserine Lactone Causes Direct Cytotoxicity and Reduced Cell Motility in Human Pancreatic Carcinoma Cells. *PLoS ONE* 9(9):e106480.

31. Hazelbauer GL, Lai W-C (2010) Bacterial chemoreceptors: providing enhanced features to two-component signaling. *Curr Opin Microbiol* 13(2):124–132.

32. Bilwes AM, Alex LA, Crane BR, Simon MI (1999) Structure of CheA, a Signal-Transducing Histidine Kinase. *Cell* 96(1):131–141.

33. Park S-Y, Beel BD, Simon MI, Bilwes AM, Crane BR (2004) In different organisms, the mode of interaction between two signaling proteins is not necessarily conserved. *Proc Natl Acad Sci U S A* 101(32):11646–11651.

34. Quezada CM, Gradinaru C, Simon MI, Bilwes AM, Crane BR (2004) Helical shifts generate two distinct conformers in the atomic resolution structure of the CheA phosphotransferase domain from Thermotoga maritima. *J Mol Biol* 341(5):1283–1294.

35. Gegner JA, Dahlquist FW (1991) Signal transduction in bacteria: CheW forms a reversible complex with the protein kinase CheA. *Proc Natl Acad Sci U S A* 88(3):750–754.

36. Gegner JA, Graham DR, Roth AF, Dahlquist FW (1992) Assembly of an MCP receptor, CheW, and kinase CheA complex in the bacterial chemotaxis signal transduction pathway. *Cell* 70(6):975–982.

37. Boukhvalova MS, Dahlquist FW, Stewart RC (2002) CheW binding interactions with CheA and Tar. Importance for chemotaxis signaling in Escherichia coli. *J Biol Chem* 277(25):22251–22259.

38. Blair DF (1995) How bacteria sense and swim. *Annu Rev Microbiol* 49. doi:10.1146/annurev.mi.49.100195.002421.

39. Halkides CJ, et al. (2000) The 1.9 Å Resolution Crystal Structure of Phosphono-CheY, an Analogue of the Active Form of the Response Regulator, CheY†,‡. *Biochemistry (Mosc)* 39(18):5280–5286.

40. Lee S-Y, et al. (2001) Crystal structure of an activated response regulator bound to its target. *Nat Struct Mol Biol* 8(1):52–56.

41. Lee S-Y, et al. (2001) Crystal Structure of Activated CheY: COMPARISON WITH OTHER ACTIVATED RECEIVER DOMAINS. *J Biol Chem* 276(19):16425–16431.

42. Zhao R, Collins EJ, Bourret RB, Silversmith RE (2002) Structure and catalytic mechanism of the E. coli chemotaxis phosphatase CheZ. *Nat Struct Biol* 9(8):570–575.

43. Simms SA, Stock AM, Stock JB (1987) Purification and characterization of the S-adenosylmethionine:glutamyl methyltransferase that modifies membrane chemoreceptor proteins in bacteria. *J Biol Chem* 262(18):8537–8543.

44. Djordjevic S, Stock AM Crystal structure of the chemotaxis receptor methyltransferase CheR suggests a conserved structural motif for binding S-adenosylmethionine. *Structure* 5(4):545–558.

45. Djordjevic S, Stock AM (1998) Chemotaxis receptor recognition by protein methyltransferase CheR. *Nat Struct Mol Biol* 5(6):446–450.

46. Lupas A, Stock J (1989) Phosphorylation of an N-terminal regulatory domain activates the CheB methylesterase in bacterial chemotaxis. *J Biol Chem* 264(29):17337–17342.

47. Djordjevic S, Goudreau PN, Xu Q, Stock AM, West AH (1998) Structural basis for methylesterase CheB regulation by a phosphorylation-activated domain. *Proc Natl Acad Sci* 95(4):1381–1386.

48. Koretke KK, Lupas AN, Warren PV, Rosenberg M, Brown JR (2000) Evolution of Two-Component Signal Transduction. *Mol Biol Evol* 17(12):1956–1970.

49. Ulrich LE, Koonin EV, Zhulin IB (2005) One-component systems dominate signal transduction in prokaryotes. *Trends Microbiol* 13(2):52–56.

50. Wuichet K, Cantwell BJ, Zhulin IB (2010) Evolution and phyletic distribution of two-component signal transduction systems. *Curr Opin Microbiol* 13(2):219–225.

51. Capra EJ, Laub MT (2012) Evolution of Two-Component Signal Transduction Systems. *Annu Rev Microbiol* 66(1):325–347.

52. Feng X, Baumgartner JW, Hazelbauer GL (1997) High- and low-abundance chemoreceptors in Escherichia coli: differential activities associated with closely related cytoplasmic domains. *J Bacteriol* 179(21):6714–6720.

53. Barnakov AN, Barnakova LA, Hazelbauer GL (1998) Comparison in vitro of a high- and a low-abundance chemoreceptor of Escherichia coli: similar kinase activation but different methyl-accepting activities. *J Bacteriol* 180(24):6713–6718.

54. Englert DL, Adase CA, Jayaraman A, Manson MD (2010) Repellent Taxis in Response to Nickel Ion Requires neither Ni2+ Transport nor the Periplasmic NikA Binding Protein. *J Bacteriol* 192(10):2633–2637.

55. Bibikov SI, Biran R, Rudd KE, Parkinson JS (1997) A signal transducer for aerotaxis in Escherichia coli. *J Bacteriol* 179(12):4075–4079.

56. Rebbapragada A, et al. (1997) The Aer protein and the serine chemoreceptor Tsr independently sense intracellular energy levels and transduce oxygen, redox, and energy signals for Escherichia coli behavior. *Proc Natl Acad Sci* 94(20):10541–10546.

57. Bray D, Levin MD, Morton-Firth CJ (1998) Receptor clustering as a cellular mechanism to control sensitivity. *Nature* 393(6680):85–88.

58. Kim KK, Yokota H, Kim S-H (1999) Four-helical-bundle structure of the cytoplasmic domain of a serine chemotaxis receptor. *Nature* 400(6746):787–792.

59. Boldog T, Grimme S, Li M, Sligar SG, Hazelbauer GL (2006) Nanodiscs separate chemoreceptor oligomeric states and reveal their signaling properties. *Proc Natl Acad Sci* 103(31):11509–11514.

60. Khan S, Spudich JL, McCray JA, Trentham DR (1995) Chemotactic signal integration in bacteria. *Proc Natl Acad Sci* 92(21):9757–9761.

61. Ames P, Studdert CA, Reiser RH, Parkinson JS (2002) Collaborative signaling by mixed chemoreceptor teams in Escherichia coli. *Proc Natl Acad Sci* 99(10):7060–7065.

62. Kim S-H, Wang W, Kim KK (2002) Dynamic and clustering model of bacterial chemotaxis receptors: Structural basis for signaling and high sensitivity. *Proc Natl Acad Sci* 99(18):11611–11615.

63. Lamanna AC, et al. (2002) Conserved Amplification of Chemotactic Responses through Chemoreceptor Interactions. *J Bacteriol* 184(18):4981–4987.

64. Maddock, Shapiro L (1993) Polar location of the chemoreceptor complex in the Escherichia coli cell. *Science* 259(5102):1717–1723.

65. Gestwicki JE, et al. (2000) Evolutionary Conservation of Methyl-Accepting Chemotaxis Protein Location in Bacteria andArchaea. *J Bacteriol* 182(22):6499–6502.

66. Sourjik V, Berg HC (2000) Localization of components of the chemotaxis machinery of Escherichia coli using fluorescent protein fusions. *Mol Microbiol* 37(4):740–751.

67. Shimizu TS, et al. (2000) Molecular model of a lattice of signalling proteins involved in bacterial chemotaxis. *Nat Cell Biol* 2(11):792–796.

68. Zhang P, Khursigara CM, Hartnell LM, Subramaniam S (2007) Direct visualization of Escherichia coli chemotaxis receptor arrays using cryo-electron microscopy. *Proc Natl Acad Sci* 104(10):3777–3781.

69. Briegel A, et al. (2009) Universal architecture of bacterial chemoreceptor arrays. *Proc Natl Acad Sci*. Available at: http://www.pnas.org/content/early/2009/09/23/0905181106.abstract.

70. Liu J, et al. (2012) Molecular architecture of chemoreceptor arrays revealed by cryoelectron tomography of Escherichia coli minicells. *Proc Natl Acad Sci*. Available at: http://www.pnas.org/content/early/2012/05/02/1200781109.abstract.

71. Krikos A, Mutoh N, Boyd A, Simon MI (1983) Sensory transducers of E. coli are composed of discrete structural and functional domains. *Cell* 33(2):615–622.

72. Milburn M, et al. (1991) Three-dimensional structures of the ligand-binding domain of the bacterial aspartate receptor with and without a ligand. *Science* 254(5036):1342–1347.

73. Hulko M, et al. (2006) The HAMP Domain Structure Implies Helix Rotation in Transmembrane Signaling. *Cell* 126(5):929–940.

74. Airola MV, Watts KJ, Bilwes AM, Crane BR (2010) Structure of concatenated HAMP domains provides a mechanism for signal transduction. *Struct Lond Engl 1993* 18(4):436–448.

75. Parkinson JS (2010) Signaling Mechanisms of HAMP Domains in Chemoreceptors and Sensor Kinases. *Annu Rev Microbiol* 64(1):101–122.

76. Starrett DJ, Falke JJ (2005) Adaptation Mechanism of the Aspartate Receptor: Electrostatics of the Adaptation Subdomain Play a Key Role in Modulating Kinase Activity†. *Biochemistry (Mosc)* 44(5):1550–1560.

77. Coleman MD, Bass RB, Mehan RS, Falke JJ (2005) Conserved Glycine Residues in the Cytoplasmic Domain of the Aspartate Receptor Play Essential Roles in Kinase Coupling and On−Off Switching†. *Biochemistry (Mosc)* 44(21):7687–7695.

78. Chervitz SA, Falke JJ (1996) Molecular mechanism of transmembrane signaling by the aspartate receptor: a model. *Proc Natl Acad Sci* 93(6):2545–2550.

79. Park S-Y, et al. (2006) Reconstruction of the chemotaxis receptor-kinase assembly. *Nat Struct Mol Biol* 13(5):400–407.

80. Wu J, Li J, Li G, Long DG, Weis RM (1996) The Receptor Binding Site for the Methyltransferase of Bacterial Chemotaxis Is Distinct from the Sites of Methylation†. *Biochemistry (Mosc)* 35(15):4984–4993.

81. Barnakov AN, Barnakova LA, Hazelbauer GL (1999) Efficient adaptational demethylation of chemoreceptors requires the same enzyme-docking site as efficient methylation. *Proc Natl Acad Sci* 96(19):10667–10672.

82. Bourret RB, Hess JF, Simon MI (1990) Conserved aspartate residues and phosphorylation in signal transduction by the chemotaxis protein CheY. *Proc Natl Acad Sci U S A* 87(1):41–45.

83. McEvoy MM, Hausrath AC, Randolph GB, Remington SJ, Dahlquist FW (1998) Two binding modes reveal flexibility in kinase/response regulator interactions in the bacterial chemotaxis pathway. *Proc Natl Acad Sci U S A* 95(13):7333–7338.

84. Briegel A, et al. (2012) Bacterial chemoreceptor arrays are hexagonally packed trimers of receptor dimers networked by rings of kinase and coupling proteins. *Proc Natl Acad Sci U S A* 109(10):3766–3771.

85. Baker MD, Wolanin PM, Stock JB (2006) Signal transduction in bacterial chemotaxis. *BioEssays News Rev Mol Cell Dev Biol* 28(1). doi:10.1002/bies.20343.

86. Parkinson JS, Hazelbauer GL, Falke JJ Signaling and sensory adaptation in Escherichia coli chemoreceptors: 2015 update. *Trends Microbiol* 23(5):257–266.

87. Segall JE, Manson MD, Berg HC (1982) Signal processing times in bacterial chemotaxis. *Nature* 296(5860):855–857.

88. Vaknin A, Berg HC (2007) Physical Responses of Bacterial Chemoreceptors. *J Mol Biol* 366(5):1416–1423.

89. Kehry MR, Dahlquist FW Adaptation in bacterial chemotaxis: CheB-dependent modification permits additional methylations of sensory transducer proteins. *Cell* 29(3):761–772.

90. Kehry MR, Bond MW, Hunkapiller MW, Dahlquist FW (1983) Enzymatic deamidation of methyl-accepting chemotaxis proteins in Escherichia coli catalyzed by the cheB gene product. *Proc Natl Acad Sci U S A* 80(12):3599–3603.

91. Springer WR, Koshland DEJ (1977) Identification of a protein methyltransferase as the cheR gene product in the bacterial sensing system. *Proc Natl Acad Sci U S A* 74(2):533–537.

92. Borkovich KA, Alex LA, Simon MI (1992) Attenuation of sensory receptor signaling by covalent modification. *Proc Natl Acad Sci U S A* 89(15):6756–6760.

93. Bornhorst JA, Falke JJ (2003) Quantitative Analysis of Aspartate Receptor Signaling Complex Reveals that the Homogeneous Two-state Model is Inadequate: Development of a Heterogeneous Two-state Model. *J Mol Biol* 326(5):1597–1614.

94. Mello BA, Tu Y (2003) Quantitative modeling of sensitivity in bacterial chemotaxis: the role of coupling among different chemoreceptor species. *Proc Natl Acad Sci U S A* 100(14):8223–8228.

95. Tu Y (2013) Quantitative Modeling of Bacterial Chemotaxis: Signal Amplification and Accurate Adaptation. *Annu Rev Biophys* 42(1):337–359.

96. Ullrich A, Schlessinger J Signal transduction by receptors with tyrosine kinase activity. *Cell* 61(2):203–212.

97. Spiegel AM (1996) Defects in G protein-coupled signal transduction in human disease. *Annu Rev Physiol* 58:143–170.

98. Uings IJ, Farrow SN (2000) Cell receptors and cell signalling. *Mol Pathol* 53(6):295–299.

99. Ottemann KM, Xiao W, Shin Y-K, Koshland DE (1999) A Piston Model for Transmembrane Signaling of the Aspartate Receptor. *Science* 285(5434):1751–1754.

100. Murphy OJ, Kovacs FA, Sicard EL, Thompson LK (2001) Site-Directed Solid-State NMR Measurement of a Ligand-Induced Conformational Change in the Serine Bacterial Chemoreceptor†. *Biochemistry (Mosc)* 40(5):1358–1366.

101. Swain KE, Gonzalez MA, Falke JJ (2009) Engineered Socket Study of Signaling through a Four-Helix Bundle: Evidence for a Yin−Yang Mechanism in the Kinase Control Module of the Aspartate Receptor. *Biochemistry (Mosc)* 48(39):9266–9277.

102. Zhou Q, Ames P, Parkinson JS (2009) Mutational analyses of HAMP helices suggest a dynamic bundle model of input-output signalling in chemoreceptors. *Mol Microbiol* 73(5):801–814.

103. Zhou Q, Ames P, Parkinson JS (2011) Biphasic control logic of HAMP domain signalling in the Escherichia coli serine chemoreceptor. *Mol Microbiol* 80(3):596–611.

104. Airola MV, et al. (2013) HAMP Domain Conformers That Propagate Opposite Signals in Bacterial Chemoreceptors. *PLoS Biol* 11(2):e1001479.

105. Koshy SS, Li X, Eyles SJ, Weis RM, Thompson LK (2014) Hydrogen Exchange Differences between Chemoreceptor Signaling Complexes Localize to Functionally Important Subdomains. *Biochemistry (Mosc)* 53(49):7755–7764.

106. Samanta D, Borbat PP, Dzikovski B, Freed JH, Crane BR (2015) Bacterial chemoreceptor dynamics correlate with activity state and are coupled over long distances. *Proc Natl Acad Sci U S A* 112(8):2455–2460.

107. Piasta KN, Ulliman CJ, Slivka PF, Crane BR, Falke JJ (2013) Defining a Key Receptor-CheA Kinase Contact and Elucidating Its Function in the Membrane-Bound Bacterial Chemosensory Array: A Disulfide Mapping and TAM-IDS Study. *Biochemistry (Mosc)* 52(22):3866–3880.

108. Gloor SL, Falke JJ (2009) Thermal Domain Motions of CheA Kinase in Solution: Disulfide Trapping Reveals the Motional Constraints Leading to Trans-autophosphorylation†. *Biochemistry (Mosc)* 48(16):3631–3644.

109. Briegel A, et al. (2013) The mobility of two kinase domains in the Escherichia coli chemoreceptor array varies with signalling state. *Mol Microbiol* 89(5):831–841.

110. Todd AP, Cong J, Levinthal F, Levinthal C, Hubbell WL (1989) Site-directed mutagenesis of colicin E1 provides specific attachment sites for spin labels whose spectra are sensitive to local conformation. *Proteins* 6(3):294–305.

111. Klug CS, Feix JB (2008) Methods and Applications of Site-Directed Spin Labeling EPR Spectroscopy. *Methods in Cell Biology* (Academic Press), pp 617–658.

112. Jeschke G (2012) DEER distance measurements on proteins. *Annu Rev Phys Chem* 63:419–446.

113. Borbat P, Freed J (2013) Pulse Dipolar Electron Spin Resonance: Distance Measurements. *Structural Information from Spin-Labels and Intrinsic Paramagnetic Centres in the Biosciences*, Structure and Bonding., eds Timmel CR, Harmer JR (Springer Berlin Heidelberg), pp 1–82.

114. Milov AD, Ponomarev AB, Tsvetkov YD (1984) Electron-electron double resonance in electron spin echo: Model biradical systems and the sensitized photolysis of decalin. *Chem Phys Lett* 110(1):67–72.

115. Chiang Y-W, Borbat PP, Freed JH (2005) The determination of pair distance distributions by pulsed ESR using Tikhonov regularization. *J Magn Reson* 172(2):279–295.

116. Chiang Y-W, Borbat PP, Freed JH (2005) Maximum entropy: A complement to Tikhonov regularization for determination of pair distance distributions by pulsed ESR. *J Magn Reson* 177(2):184–196.

117. Pannier M, Veit S, Godt A, Jeschke G, Spiess H. (2000) Dead-Time Free Measurement of Dipole–Dipole Interactions between Electron Spins. *J Magn Reson* 142(2):331–340.

Chapter Two

Bacterial chemoreceptor dynamics correlate with activity state and are coupled over long distances

2.1 Introduction:

The ability of localized dynamics to modulate the function of transmembrane receptors is an emerging theme in signal transduction (1-4). These ideas have been largely supported by computational studies (2), although direct measurements also correlate dynamics with activity (1-4). Nonetheless, we are only beginning to address the link between conformational heterogeneity and signal propagation in complex proteins. Bacterial chemotaxis, the process by which cells modulate their motility in response to the chemical environment, provides an important model system to explore receptor dynamics experimentally (5, 6). During chemotaxis, attractant-bound chemoreceptors cause counterclockwise (CCW) flagella rotation and smooth swimming, whereas repellant-bound receptors cause clockwise (CW) flagella rotation and cell tumbling. Chemoreceptors, also termed methyl-accepting chemotaxis proteins (MCPs) form extended arrays in the cytoplasmic membrane to communicate ligand binding (6) to the histidine kinase CheA and the coupling protein CheW. Great progress has been made in understanding how receptors communicate ligand binding events across the cytoplasmic membrane, but how these changes affect CheA is not well understood (5-7).

Homodimeric chemoreceptors have a modular architecture. Each subunit supplying a periplasmic ligand binding domain, a helical transmembrane region and half of two cytoplasmic 4-helix bundles that extend from the membrane to engage CheA and CheW in the cytoplasm (8). The transmembrane region contains four antiparallel helices (TM1/TM2, TM1'/TM2') and connects to the membrane-proximal HAMP domain through TM2 and TM2'. The HAMP domain (for **H**istidine kinase, **A**denylyl cyclases, **M**ethyl accepting chemotaxis proteins, and **P**hosphatases) comprises a parallel 4-helix bundle (AS1/AS2, AS1'/AS2')

with two helices supplied from each subunit (7). HAMP joins to the kinase-control module (KCM), which forms a long, antiparallel 4-helix bundle, also with two helices supplied by each subunit (CD1/CD2 and CD1'/CD2') (6). The KCM can be further divided into an adaptation region, a flexible bundle with glycine hinge and a protein interaction region (PIR) at the receptor tip. The adaptation region contains conserved Glu residues that undergo reversible methylation/demethylation by the methylase CheR and methylesterase CheB, respectively. For the well-studied aspartate (Tar) and serine (Tsr) receptors of *E. coli*, chemoattractant binding inhibits CheA activity (kinase-off, CCW flagellar rotation) and this effect is countered by methylation, which reactivates the kinase and weakens affinity for attractant. In contrast, binding of repellants (or release of attractant) activates CheA (kinase-on, CW flagellar rotation) and is similarly countered by demethylation. Substitution of specific Glu residues to Gln functionally mimics methylation (9).

Conformational changes associated with ligand binding to chemoreceptors are well described in the periplasm and transmembrane regions (6, 8, 10), but less so in the cytoplasm. Attractant binding to the periplasmic domain of Tar causes a vertical displacement of the a4 helix that directly attaches to TM2 (10). TM2 responds with a piston displacement that has been characterized by a variety of experimental and computational methods (6, 8, 11, 12). The TM2 piston motion relays to the HAMP domain through a small "control cable" on the cytoplasmic side of the membrane (13). HAMP is then proposed to undergo a change in both structure and dynamics (7, 14). Mutagenesis studies suggest that HAMP in kinase-off states is less dynamic than in kinase-on states (7, 15, 16). Molecular dynamics simulations on membrane embedded Tar provide a different picture, wherein ligand binding produces only modest changes in dynamics, with motions of AS2 slightly increasing in the kinase-off state (12). Dynamical changes in HAMP may be mirrored by dynamical changes in the KCM: mutations that destabilize packing in the PIR lock-in kinase-on states, whereas destabilization of the adaptation region produces kinase-off states (17). Rates of disulfide cross-linking indicate that kinase-off mutations are indeed more dynamic (14, 17). This

so-called “yin-yang” model (14) represents the cytoplasmic regions of the receptor as two units – the adaptation and PIRs - which alternate their degree of conformational fluctuation depending on signaling state (14). Between these modules, a flexible bundle region facilitates conformational coupling (18).

Structural changes within the KCM have also been attributed with kinase regulation. The HAMP AS2 helices may undergo a scissor opening motion when transitioning from kinase-off to kinase-on (14, 19). Attractant sensitive disulfide bond formation between CheA and receptor suggest that the N-terminal CD1 helices rotate in the PIR upon ligand binding (20). Rotations (21, 22) and longitudinal shifts of helices (23) within HAMP have been implicated as regulatory switches and such transitions may interconvert states with different dynamical properties. Long duration, all-atom molecular dynamics simulations indicate that separation of one KCM N-terminal helix (CD1) and the C-terminal helix of the other subunit (CD2’) are coupled to the flipping of a conserved Phe residue at the receptor tip and that these changes correlate with modification state (24). Nonetheless, these observations have yet to be combined in an encompassing model of receptor activation.

We have shown that when two structurally distinct HAMP modules (H1 or H1-2) taken from *P. aerurginosa* Aer2 are fused to the Tar KCM, the resulting chimeras produce exclusive kinase-on and kinase-off states in cells (25). Pulsed-dipolar ESR spectroscopy (PDS) in concert with site-specific spin labeling (SDSL) demonstrated that the two HAMP modules maintained their structures in the respective fusions and further enforced their AS2 arrangements across the junction into the KCM (25). The activating HAMP (H1) indeed displayed much broader distributions of spin separations than the inactivating module (H1-2) and these dynamical features were mirrored in the attached KCM. Here we further employ PDS and CW-ESR to probe the KCM dynamics of these kinase-on (H1-Tar) and kinase-off (H1-2-Tar) effector modules (Fig. 2-1). The widths of PDS distance distributions correlate well with spin-label dynamics. Together they reveal that in a given effector, the HAMP domain enforces a similar helical

separation, and dynamic state across the junction into the KCM, whereas the PIR assumes the opposite behavior. The conformational dynamics and activation state of all modules coherently switch when H1 is replaced by H1-2 and these changes can be mostly reversed by covalent modification in the adaptation region.

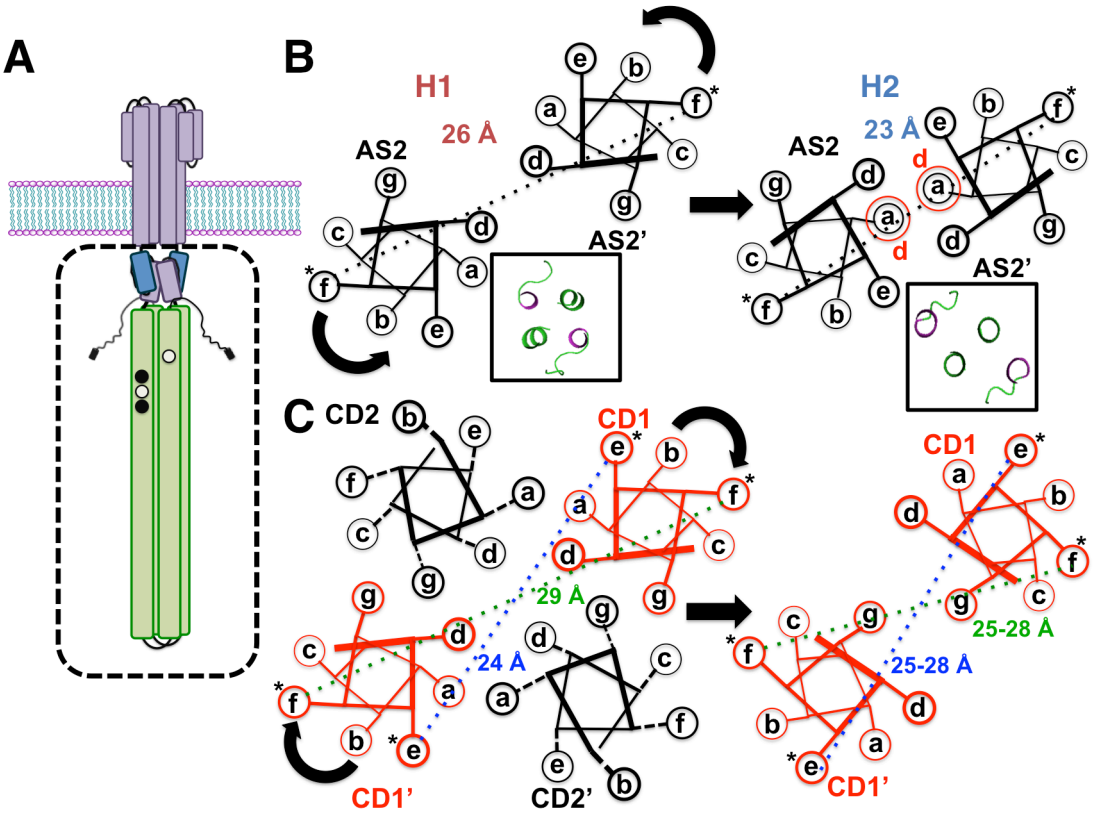

Figure 2-1: Schematic representations of spin-separations generated by different helix packing and labeling locations. (A) Schematic of the bacterial chemoreceptor is shown, with the effector module, studied in this report, depicted in box. (B) Differences in spin separations on AS2 between the H1 and H1-2 conformations predicted from their crystal structures. Insets display the crystal structure of the C-terminal plane of the two HAMPs viewed from the N-terminal end (AS2, and linker in green). (C) Differences in spin-separations within the 4-helix bundle of the KCM for an f and e site (with * representing the spin label) and the hypothetical effect of a CW CD1 rotation on these distances.

2.2 Results:

2.2.1 CheA activity and ternary complex stability:

Aer2 contains a poly-HAMP module of three concatenated HAMP domains (H1-2-3). The structure of the H1-2-3 poly-HAMP revealed that H2 has a different conformation compared to H1 and H3, which are similar in structure (26). In H2, the bundle is rhombically distorted such that the AS2 helices interact more closely and approximate a two-helix coiled-coil (Fig. 2-1B). As previously reported (25), chimeras that fuse H1 to the Tar KCM (here H1-Tar, named H1s in (25)) and H1-2 to the Tar KCM (here H1-2-Tar, named H1-2s in (25)) produce very different output signals when expressed in *E. coli* cells devoid of all other receptors (Fig. 2-2A). In cells lacking the adaptation system (CheRB-) H1-Tar is 100% CW (kinase-on) and H1-2-Tar is almost exclusively CCW (kinase-off). In the presence of the methylation system (CheRB+), kinase activation increases with H1-2-Tar, although a converse inhibition is not seen with H1-Tar.

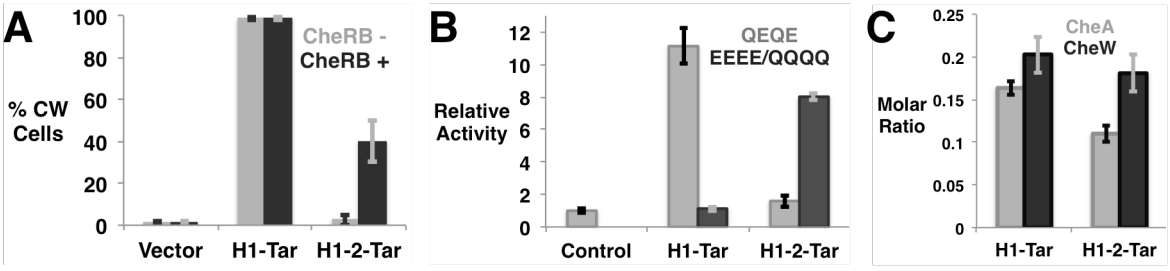

Figure 2-2: Properties of the H1-Tar and H1-2-Tar effectors. (A) ***In vivo* activity of H1-Tar and H1-2-Tar.** Expression of H1-Tar and H1-2-Tar in an *E.coli* strain devoid of other receptors gives different cell swimming behavior, which reflects their ability to activate CheA. The tumbling frequency was measured in adaptation less background (CheRB -, grey bars) as well as with adaptation proteins present in the cell (CheRB +, black bars). The bars plot the median, and the error bars border the lower and upper limit of the ranges of tumbling frequency observed (Adapted from (1)). Vector alone serves as the control. (B) ***In vitro* activity of H1-Tar and H1-2-Tar.** H1-Tar (grey) stimulates the phosphotransfer activity of CheA to CheY relative to CheA and CheW alone (control), whereas H1-2-Tar (grey) does not. This difference in activity is largely

reversed upon covalent modification in H1-Tar EEEE (black), or H1-2-Tar QQQQ (black). Error bars represent standard errors of the mean (SEM) calculated from at least four independent experiments (4≤n≤6). (C) **Interaction of H1-Tar and H1-2-Tar with CheA and CheW.** Purified CheA and CheW were pulled down with S-tagged effectors. Molar subunit ratios of bound CheA and CheW to effector were calculated as described in the methods section, and averaged from five independent experiments. Error bars are shown as SEMs (n = 5; P = 0.01 and P = 0.06 for differential binding of CheA and CheW, respectively).

In vitro assays demonstrate the ability of H1-Tar and H1-2-Tar to differentially regulate CheA phosphotransfer activity without appreciably altering binding to the kinase or CheW (Fig. 2-2). H1-Tar activates phosphotransfer to CheY over 10 fold, whereas H1-2-Tar does not (Fig. 2-2B). These effects are largely reversed by modification in the adaptation region: when all Gln sites in H1-Tar are changed to Glu (EEEE), H1-Tar no longer activates CheA and when the H1-2-Tar sites are changed to Gln (QQQQ) phosphotransfer increases substantially (Fig. 2-2B). Pull-down experiments with affinity tagged effectors and purified *E. coli* CheA and CheW show that the opposing *in vitro* and cellular activities of H1-Tar and H1-2-Tar in the same modification state (QEQE) do not derive from the ability of only one protein to produce ternary complexes. Both effectors bind similar amounts of CheA and CheW with H1-Tar binding slightly more of both proteins (Fig. 2-2C). The molar subunit ratios in the pull-downs of receptor:CheW:CheA are [6:1.2:1] for H1-Tar and [6 :1.1:0.7] for H1-2-Tar, which in both cases are quite close to the stoichiometry predicted for the membrane arrays [6:1:1] (27, 28).

2.2.2 Conformational differences in the KCM:

PDS and SDSL were used to report on conformational dynamics at the HAMP junction and throughout the KCM (Fig. 2-3). Engineered Cys residues were spin-labeled with nitroxides (MTSL) on HAMP AS2 and at seven sites in the KCM (Fig. 2-3). Distance distributions between each spin pair generated by effector dimerization were measured for both H1-Tar and H1-2-Tar by the PDS technique

of DEER spectroscopy (Fig. 2-3; Table 2-1) (29). Broader spatial distributions represent larger amplitude motions of the spin-labels. Residues in the H1 and H1-2 Aer2 HAMP domains have their Aer2 numbering, whereas residues in KCM have their *E. coli* Tar values. R53 of H1-Tar and A109 of H1-2-Tar are equivalent positions at the C-terminal end of AS2 in the respective HAMP modules. E270, in N-terminal helix CD1, resides across the junction into the KCM at the HAMP proximal end of adaptation region. A298 resides in CD1 and A487 resides in CD2 of the adaptation region. A312 (in CD1) and A417 (in CD2) border the flexible bundle region. I375 and A381 (in CD1/CD1') are in the N-terminal helix of the PIR. These positions were chosen to be mostly "f" sites in the heptad repeats of the effector coiled-coils to minimize any structural perturbation by the label (although A381 holds an "e" site; Fig. 2-1C). Indeed, spin-labeling the effectors in the HAMP and adaptation region does not affect their activities (Fig. 2-4).

The PDS distance distributions report on conformational differences in the helices through their mean values and reflect on dynamics through their breadth (see Fig. 2-1). For example, because the H2 structure approximates a two-helix coiled-coil, with the AS2 helices more closely associated than in H1, PDS finds that the 53 distribution has greater mean (26 Å) than the 109 distribution (23 Å) (Fig. 2-1B, Fig. 2-3). Indeed, the short H2 distribution is sharply bimodal due to either distinct helix or spin-label conformations. The spin separations are mirrored across the junction into the KCM: the 270 position in H1-Tar shows a broad distribution centered at ~30 Å, characteristic of an f position in a 4-helix bundle, but 270 in H1-2-Tar instead shows a short, sharp separation characteristic of the 2-helix packing in H2 AS2. In the adaptation region, the CD2 site (487) has a wider distribution in H1-2-Tar than in H1-Tar, but the CD1 site (298) is similar for both, and overall narrower. Through the flexible bundle region, the H1-Tar and H1-2-Tar distributions for 312 (CD1) and 417 (CD2) are nearly superimposable and typical of a dynamic 4-helix bundle. Some distributions (particularly within H1-Tar) show a second peak of lower amplitude at approximately twice the primary peak distance. These longer separations are due partly to a small contribution from disulfide cross-linked dimers (Fig. 2-6), but

may also arise from a second family of conformational states where the helices are far separated (see below). Interestingly, the second peak arises only in the HAMP domain (in some cases) and adaptation region, both of which are less-well ordered in cellular arrays viewed by cryo-EM (27).

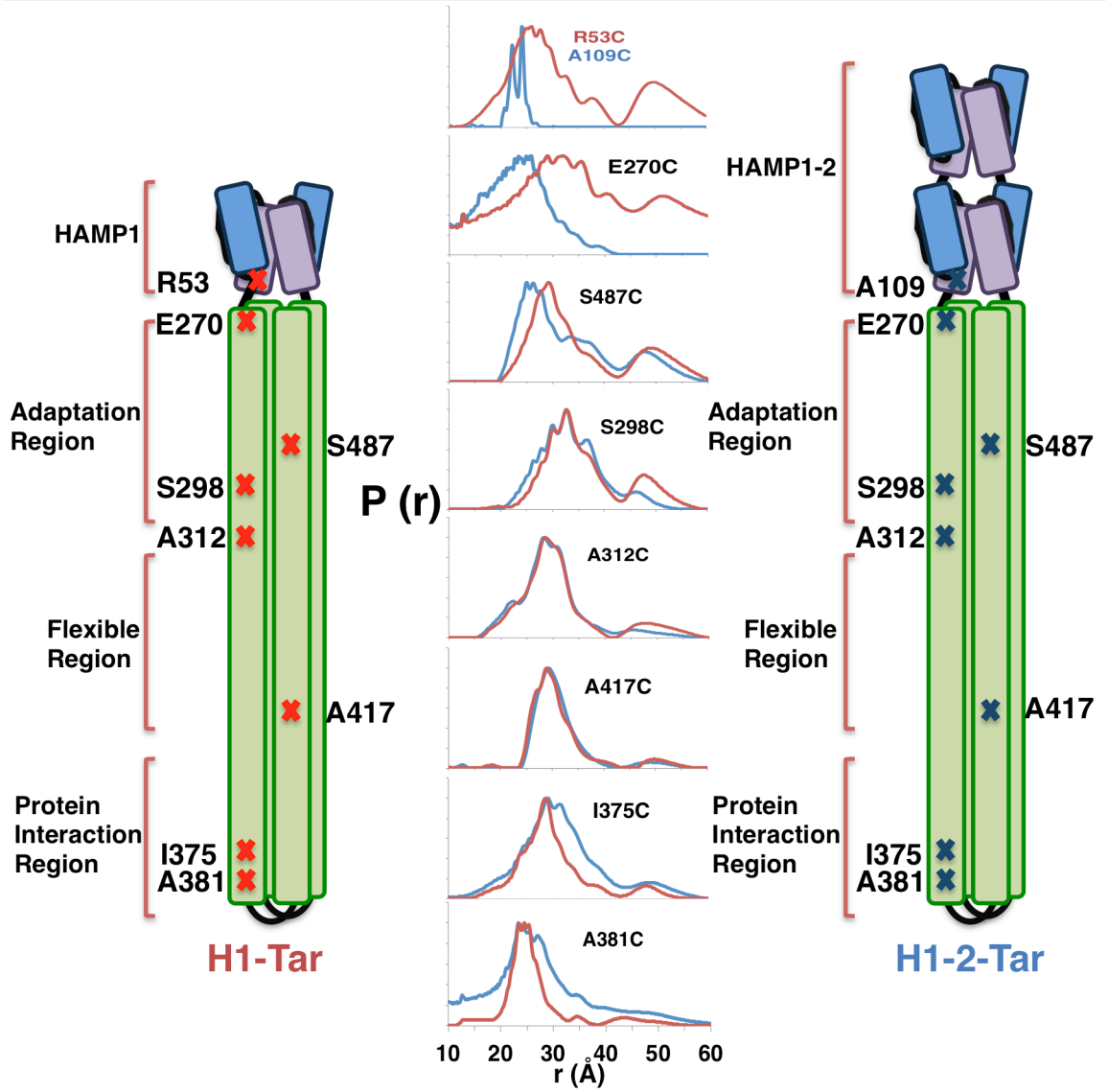

Figure 2-3: Dynamical properties of the HAMP-KCM inferred by PDS. Schematic diagrams of H1-Tar and H1-2-Tar are marked with the residues where spin labels have been introduced. Due to dimeric symmetry each spin site

position produces two spin-sites from which distance distributions across the helix bundle are measured by PDS. Distance distributions (P(r)) measured by DEER spectroscopy are shown for H1-Tar (red) and H1-2-Tar (blue), both in the QEQE adaptation state.

Residues	HAMP-Tar	r_{max} (Å)	FWHM (Å)
R53C / A109C	H1-Tar R53C	26.0	10.3
	H1-2-Tar A109C	24.2	2.9
E270C	H1-Tar	29.0	22.0
	H1-2-Tar	25.6	13.9
S487C	H1-Tar	29.2	8.4
	H1-2-Tar	25.1	7.9
S298C	H1-Tar	32.7	8.9
	H1-2-Tar	32.6	11.2
A312C	H1-Tar	28.6	7.6
	H1-2-Tar	28.3	7.6
A417C	H1-Tar	28.9	6.7
	H1-2-Tar	29.3	6.6
I375C	H1-Tar	28.7	6.6
	H1-2-Tar	29.0	11.5
A381C	H1-Tar	24.5	5.5
	H1-2-Tar	23.3	9.6

Table 2-1: Parameters of the distance distribution for each site at QEQE adaptation state. r_{max} (maximum probable distance) and FWHM (full width at half maximum) are tabulated for distane distribution at each sites in H1-Tar (white rows) and in H1-2-Tar (grey rows), both in QEQE adaptation state.

The PDS distance distributions report on conformational differences in the helices through their mean values and reflect on dynamics through their breadth

(see Fig. 2-1). For example, because the H2 structure approximates a two-helix coiled-coil, with the AS2 helices more closely associated than in H1, PDS finds that the 53 distribution has greater mean (26 Å) than the 109 distribution (23 Å) (Fig. 2-1B, Fig. 2-3). Indeed, the short H2 distribution is sharply bimodal due to either distinct helix or spin-label conformations. The spin separations are mirrored across the junction into the KCM: the 270 position in H1-Tar shows a broad distribution centered at ~30 Å, characteristic of an f position in a 4-helix bundle, but 270 in H1-2-Tar instead shows a short, sharp separation characteristic of the 2-helix packing in H2 AS2. In the adaptation region, the CD2 site (487) has a wider distribution in H1-2-Tar than in H1-Tar, but the CD1 site (298) is similar for both, and overall narrower. Through the flexible bundle region, the H1-Tar and H1-2-Tar distributions for 312 (CD1) and 417 (CD2) are nearly superimposable and typical of a dynamic 4-helix bundle. Some distributions (particularly within H1-Tar) show a second peak of lower amplitude at approximately twice the primary peak distance. These longer separations are due partly to a small contribution from disulfide cross-linked dimers (Fig. 2-6), but may also arise from a second family of conformational states where the helices are far separated (see below). Interestingly, the second peak arises only in the HAMP domain (in some cases) and adaptation region, both of which are less-well ordered in cellular arrays viewed by cryo-EM (27).

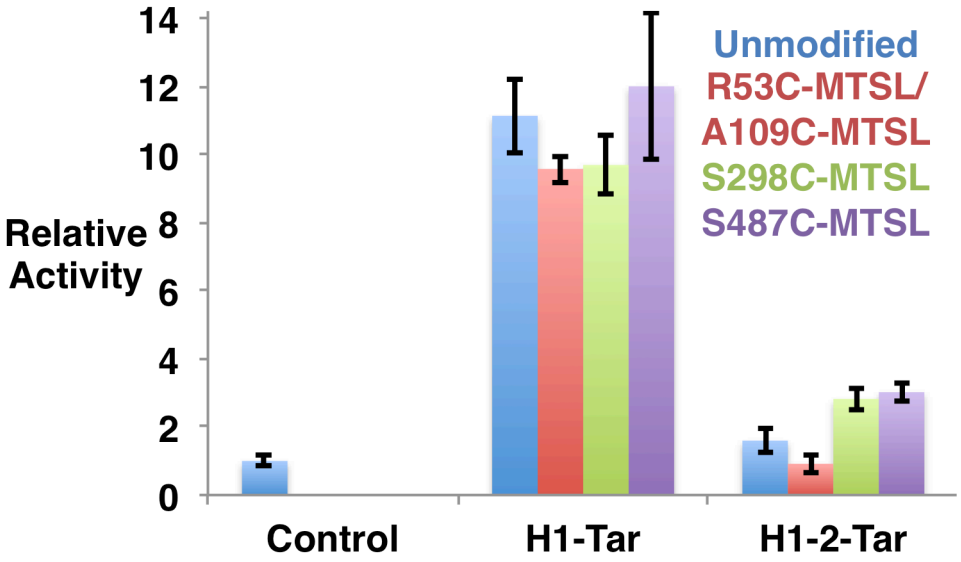

Figure 2-4: Constancy of signaling properties of mutated and spin labeled effectors: Mutations and spin labels employed in the ESR study do not alter the signaling properties of the effectors, as measured in CheY phospho-transfer assay. Standard errors of the mean (SEMs), calculated from at least three independent experiments (3≤n≤4), are presented as the error bars.

As in HAMP, the sites in the PIR (375 and 381) show quite different behavior for H1- and H1-2-Tar. Unlike HAMP, the trend in dynamics reverses, with H1-Tar having the more stable, narrow distributions and H1-2-Tar generating broader spin-spin separations indicative of increased dynamics. Thus, the measurements reveal yin-yang behavior between HAMP and the PIR, with a more mobile HAMP (kinase-on) producing a tighter PIR and visa versa (Fig. 2-3). In H1-Tar, ~25 Å mean of the 381 distribution (e position) is notably shorter than ~30 Å mean of the 375 distribution (f position), as would be predicted by the structure of a 4-helix bundle (Fig. 2-1C). Targeted disulfide cross-linking studies indicate that the CD1 helices may rotate in the kinase-off state (20) (i.e. for H1-2-Tar); this should increase the 381 separation and decrease the 375 separation in H1-2-Tar relative to that in H1-Tar (Fig. 2-1C). Interestingly, the 381 distribution does skew toward a longer distance in H1-2-Tar (Fig. 2-3), but a corresponding decrease in the 375 mean is not observed. Nonetheless, both the 375 and 381 distributions broaden in H1-2-Tar, thereby indicating that increased dynamics in the PIR is likely the dominant factor in transitioning to the kinase-off state. However, given that the sites in the Gly hinge and adaptation region also do not show changes consistent with CD1 rotation, it is unlikely such a concerted motion propagates down the entire KCM.

2.2.3 Effector modification inverts conformational dynamics:

Modification impacts CheA activation (Fig. 2-2B) and thus, we tested if spin-spin separations at different regions of the effectors respond to modification state. QQQQ and QEQE states were monitored in H1-2-Tar (QEQE = kinase-off), and the QEQE and EEEE states in H1-Tar (QEQE = kinase-on; Fig. 2-5; Table 2-2).

Increasing charge (and thus local coulomb repulsion) in H1-Tar (QEQE -> EEEE) shifts the distribution at S298 toward longer distance and greater width (Fig. 2-5A). Furthermore a second major peak appears in the distribution centered at ~50 Å.

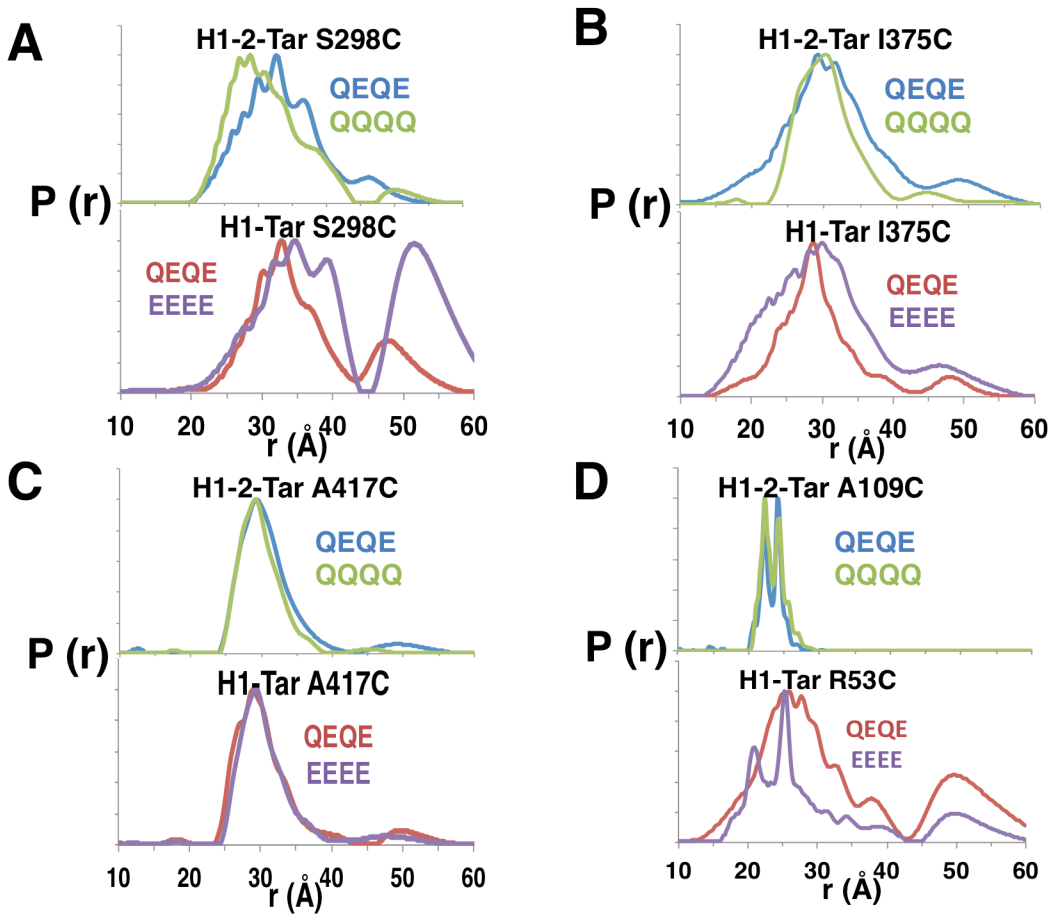

Figure 2-5: Modification of adaptation sites reveals allosteric coupling throughout the HAMP-KCM. Methylation of the effector adaptation regions was mimicked by glutamine substitution. (A) Increased modification and decreasing charge in H1-2-Tar (QQQQ) shifts the distribution at the adaptation region towards smaller distances, whereas decreased modification (EEEE) and increasing charge in H1-Tar shifts the distribution to longer distances and amplifies the peak centered around ~ 50 Å. (B) Increased modification of H1-2-Tar decreases the distance distribution (P(r)) breadth and stabilizes the PIR,

whereas in H1-Tar, decreased modification increases the P(r) breadth and destabilizes the PIR. (C) Modification at the adaptation region has no effect on PDS distributions in the hinge region for either effector. (D) Increased modification of H1-2-Tar has little effect on spin distributions in AS2 of the HAMP domain; however, decreased modification stabilizes the HAMP domain of H1-Tar toward the sharp bimodal distribution as seen in H1-2-Tar.

Examination of samples after PDS revealed only minor disulfide crosslinking (Fig. 2-6). Thus, the larger distances represent a conformation where the CD1 helices no longer pack as a 4-helix bundle. In contrast, decreasing charge in H1-2-Tar (QEQE -> QQQQ) skews the distribution at S298 toward smaller separations (Fig. 2-5A) with slightly smaller breadth (Table 2-2). This measurement provides direct evidence that increased charge due to demethylation or deamidation locally increases dynamics and destabilizes the adaptation region away from a compact 4-helix bundle. In the PIR, deamidation (QEQE -> EEEE) of H1-Tar causes I375 to become more dynamic and the HAMP site to order; indeed the distributions now resemble those of H1-2-Tar QEQE (Fig. 2-5B and 2-5D).

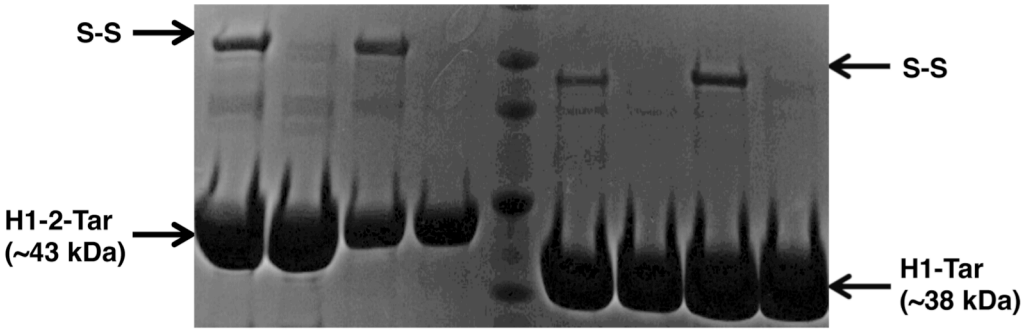

Figure 2-6: Typical SDS-PAGE analysis of DEER/CW ESR samples. The samples for DEER/ CW ESR measurement reveal the existence of disulfide cross links on SDS-PAGE gel. The disulfide links are reduced upon DTT addition. Samples for **S298C** are shown as an example in all four states. H1-2-Tar in QQQQ state, lane 1; H1-2-Tar in QQQQ state with DTT, lane 2; H1-2-Tar in QEQE state, lane 3; H1-2-Tar in QEQE state with DTT, lane 4; molecular weight marker, lane 5; H1-Tar in QEQE state, lane 6; H1-Tar in QEQE state with

DTT, lane 7; H1-Tar in EEEE state, lane 8; and H1-Tar in EEEE state with DTT, lane 9.

Remarkably, the sharp bimodal distribution of H1-2 (which represents two closely related conformations of protein and/or spin-label) is reproduced in H1-Tar EEEE. Thus, adaptation switches the H1 conformation toward that of H2. In contrast, charge neutralization (i.e. methylation QEQE->QQQQ) in H1-2-Tar causes the I375 site to become more rigid (Fig. 2-5B). However, in H1-2-Tar the HAMP site does not correspondingly shift to a more mobile state (Fig. 2-5D). This is likely because modification cannot easily overcome the high stability of the dual HAMP H1-2 unit. Surprisingly, modification in the adaptation region does not influence conformation or dynamics at the A417 site in either of the two effectors (Fig. 2-5C). Overall, adaptation mostly reverses the dynamical properties both up and down the receptor, thereby underscoring the conformational coupling throughout the entire HAMP-KCM.

Mutants	Modification	r_{max} (Å)	FWHM (Å)
H1-Tar R53C	QEQE	26.0	10.3
	EEEE	25.2	5.9
H1-2-Tar A109C	QEQE	24.2	2.9
	QQQQ	22.2	3.3
H1-Tar S298C	QEQE	32.7	8.9
	EEEE	34.6	12.3
H1-2-Tar S298C	QEQE	32.6	11.2
	QQQQ	28.9	10.6
H1-Tar A417C	QEQE	28.9	6.7
	EEEE	29.3	6.2
H1-2-Tar A417C	QEQE	29.3	6.6
	QQQQ	29.2	5.9
H1-Tar I375C	QEQE	28.7	6.6
	EEEE	29.8	15.3
H1-2-Tar I375C	QEQE	29.0	11.5
	QQQQ	30.0	8.4

Table 2-2: Comparison of the parameters of distance distributions at different adaptational states. r_{max} (maximum probable distance) and FWHM (full width at half maximum) are compiled for distane distribution at different regions in HAMP-Tar proteins with different adaptational states.

2.2.4 Dynamic measurements by CW-ESR:

Pulsed-dipolar ESR must be performed on flash-cooled samples to lengthen spin-dephasing times (29). Thus, the distance distributions measure the heterogeneity of conformational states in cold-trapped, static samples, from which dynamics prior to flash-cooling are inferred. To corroborate the relationship between dynamics and distribution width, we also measured continuous wave (CW)-ESR on liquid samples at three temperatures: 4^{o}C, 20^{o}C, and 30^{o}C. The line shapes of the solution CW ESR spectra reflect dynamics of the nitroxides on the nano-second timescale (30, 31). CW-ESR spectra of spin-labels at the HAMP (53 and 109 positions) and PIR (375) all clearly show two-component spectra (Table 2-3; Fig. 2-8). One component corresponds to a relatively immobilized state and closely approximates a rigid limit spectrum ($2A_{zz}$ is equal to ~ 69G). The rigid-like component was simulated (32) and its variable fraction subtracted from the experimental spectrum to obtain a smooth line without outer features. The subtraction reveals the shape of the second major component with faster molecular motion parameters (Fig. 2-8; Table 2-4). The fractions of these components were then calculated from double integrals. An isotropic diffusion parameter set to $R_{ll} = R_{prp} = 8x10^{6}$ s^{-1} is sufficient to produce the correct splitting value and allows for robust subtraction of the rigid, slow component to reveal the mobile fraction. The slow diffusion could reflect spin labels associated with relatively rigid helices (33). In contrast, the state with higher mobility indicates relatively free motion of the tethered spin-label and thus little constraint by the attached protein (30, 31, 34).

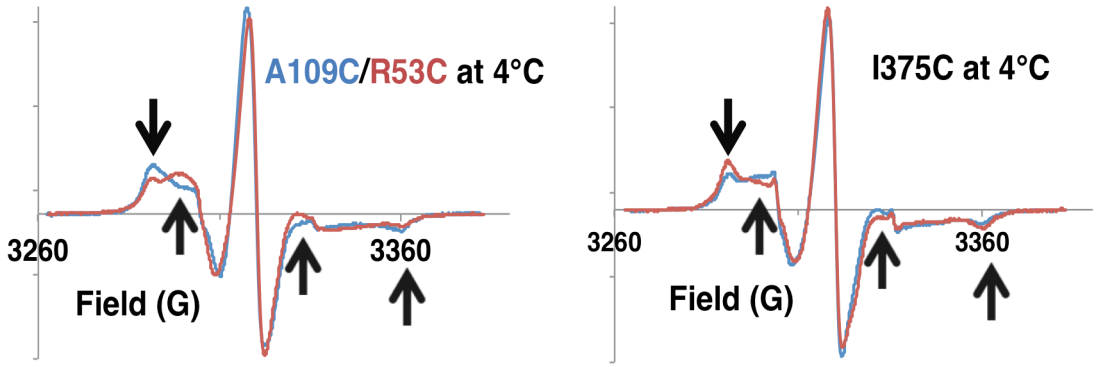

Figure 2-7: CW–ESR spectra reflect dynamic differences in HAMP and KCM. Spectra of spin labels at the HAMP domain (left panel), and PIR (right panel) reveal differences in the dynamics in H1-2-Tar (blue), and H1-Tar (red). Consistent with the PDS distributions (Fig. 2-3), the PIR is more rigid, but the HAMP domain is more dynamic, in H1-Tar. Black arrows mark the spectral regions where the differences are prominent.

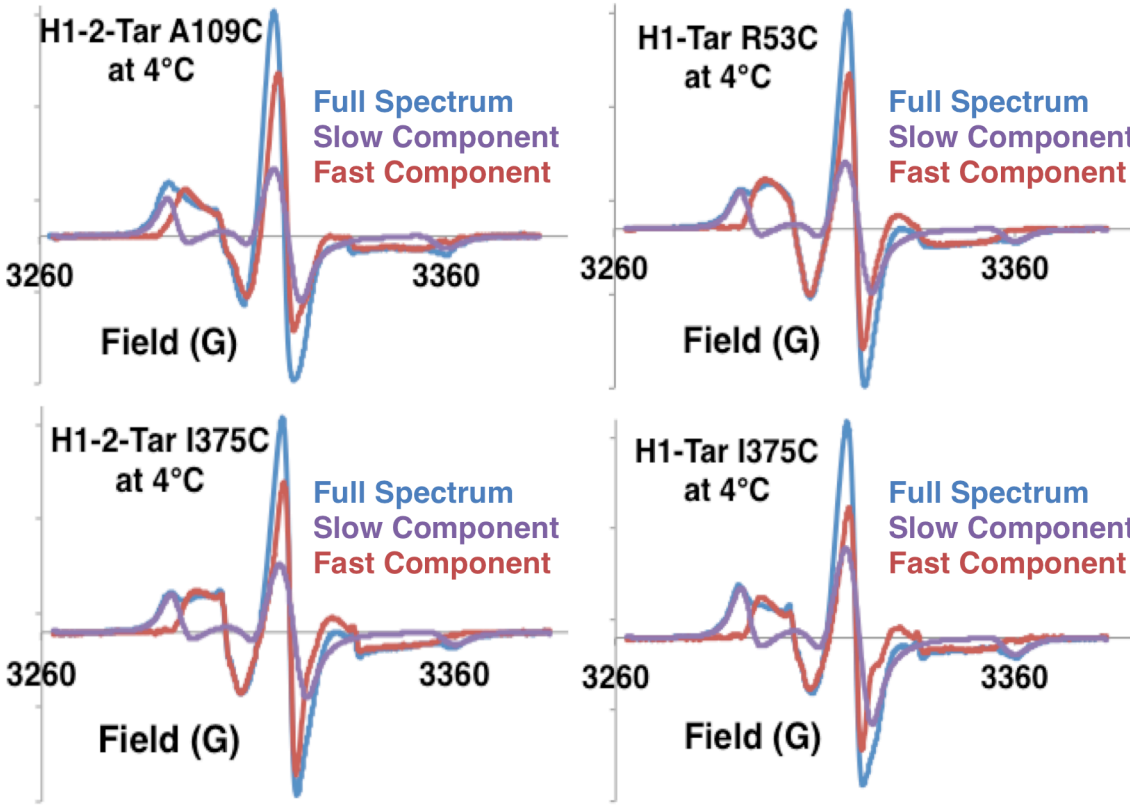

Figure 2-8: Deconvolution of the CW ESR spectra into two components. CW ESR spectra (blue) are deconvoluted into slow (purples) and fast (red) motional components.

The overall behavior of the spin-labels most likely reflects an equilibrium between states where the spin label interacts with the surface of a relatively rigid substructure, such as receptor helices (33, 35) and states where the label tumbles unencumbered by the protein (31). The increased motion could be due to the nitroxide tether releasing from the protein surface or may involve conformational transitions of the protein itself. In either case, the underlying cause of the increased mobile fraction reflects greater protein dynamics in these regions. Increase in the mobile component with temperature for all variants indicates that the rigid component is not an artifact related to, for example, partial denaturation and/or aggregation of the protein (Fig. 2-9; Table 2-3). At lower temperature, the sites with broader PDS distributions (H1-2 375, H1 53) show greater contributions from the more mobile conformation (Fig. 2-7; Table 2-3). As temperature increases, the mobile state dominates at all sites and the fractions become similar in the two effectors (Table 2-3). At the highest temperature the HAMP is generally more dynamic than the PIR and the two effectors only produce small differences at either position. Thus, the broader PDS distributions represent an ensemble of conformational states, some of which contain restrained nitroxides and others released nitroxides. At lower temperature, this ensemble coalesces into two distinct states with different spin-label dynamics on the nanosecond timescale. As the temperature increases, a range of intermediate states becomes occupied, most with relatively fast spin-label dynamics. Those sites with narrower PDS distributions (e.g. H1-375, H1-2-109) have access to a greater proportion of states with constrained nitroxides.

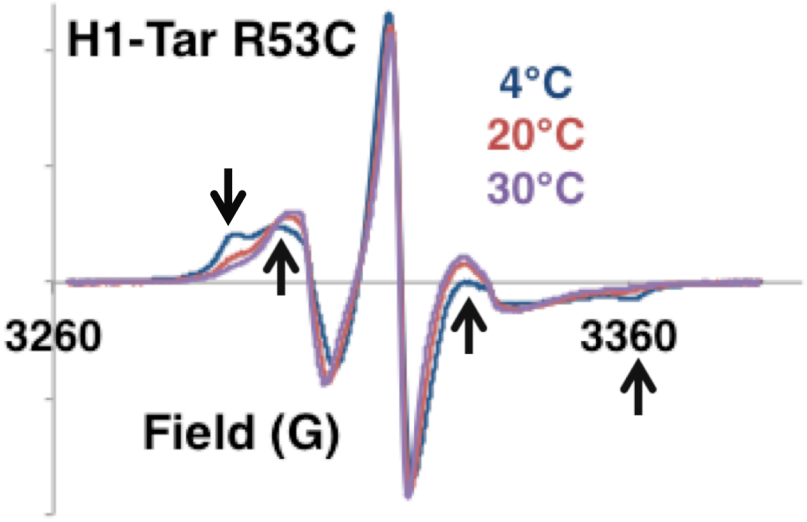

Figure 2-9: Variation of CW ESR spectra with temperature. CW ESR spectra of MTSL attached to R53C position in H1-Tar show a fraction of increased order with decreasing temperature. Black arrows mark the spectral regions where the differences are prominent.

Two-component Analysis	4°C		20°C		30°C	
	Slow	Fast	Slow	Fast	Slow	Fast
H1-2-Tar A109C	52.5%	47.5%	28.5%	71.5%	20%	80%
H1-Tar R53C	47%	53%	26.5%	73.5%	16%	84%
H1-2-Tar I375C	52%	48%	31%	69%	24%	76%
H1-Tar I375C	61%	39%	41%	59%	28%	72%

Table 2-3: Quantification of the slow and fast component from CW-ESR spectra. CW-ESR spectra for spin labels in the HAMP (109, 53) and protein interaction (375) regions were fit to two components, one representing a rigid nitroxide (slow component) and the other representing freely-rotating nitroxide (fast component), as described in main text.

Simulation Parameters for the Mobile Components	4°C		20°C		30°C	
	$Log(R_{prp})$	C_{20}	$Log(R_{prp})$	C_{20}	$Log(R_{prp})$	C_{20}
H1-2-Tar A109C	7.62	- 1.6	7.70	- 1.4	7.73	- 0.93
H1-Tar R53C	7.66	- 1.66	7.75	- 1.12	7.87	- 0.98
H1-2-Tar I375C	7.66	- 1.1	7.78	- 1.1	7.85	- 1.02
H1-Tar I375C	7.64	- 1.2	7.72	- 1.1	7.82	- 1.02

Table 2-4: Motional parameters for the mobile components. Mobility as $Log(R_{prp})$, and ordering of the attached MTSL as C_{20} are listed for all of the mobile components at various temperatures, as obtained from the simulation. $Log(R_{||})$ is set at 8.5 for all the simulations.

2.3 Discussion:

Changes in local dynamics have been linked to functionally distinct states in G-protein coupled receptors (GPCRs) (1, 2) and receptor tyrosine kinases (3). Our results confirm the modular structure of the chemoreceptor cytoplasmic domain. Although the measurements were made in the absence of membrane arrays, full-length dimeric receptors do transmit conformational signals between the ligand binding and the adaptation regions (36-38). Furthermore, H1-Tar and H1-2-Tar differentially regulate CheA phosphotransfer *in vitro* and respond appropriately to adaptation. Thus, the intrinsic properties of these effectors influence ternary complex activity, whose summed dynamics may differ from, but must be a function of, those of the individual receptors. Overall, the system displays dynamic coupling throughout, with kinase-on and kinase-off states set by either HAMP conformation or covalent modification in the adaptation region. HAMP enforces the opposite dynamical state on the PIR (Fig. 2-10). When the HAMP is conformationally destabilized (high dynamics) it is unable to influence the PIR, which sets into a more rigid state; however, when the HAMP module stabilizes, the receptor tip destabilizes and its dynamics increase. In the adaptation region, CD2 becomes more dynamic in the kinase-off state, but somewhat surprisingly CD1 shows similar distributions in both H1-Tar and H1-2-Tar. This is also true for sites in the flexible bundle region, where the spin-labels give similar distributions

in H1-Tar and H1-2-Tar. Chemical modifications of the adaptation sites produce large local effects. The EEEE state of H1-Tar markedly disorders the 298 position, but the QQQQ state of H1-2-Tar compacts the same region. CheR and CheB recognize different conformational states of the receptor (36). The large helical separation reported by the 298 site for the EEEE state is then likely CheR specific, whereas the more compact structure of the QQQQ state provides a better substrate for CheB. Although modification generally compensates for HAMP-enforced states of dynamics in these systems, reversal is not complete, which may reflect multi-state behavior in switching (39).

H1-Tar and H1-2-Tar cannot be distinguished by simple conformational transitions that involve rigid motions of the helices. Uniform helical rotations, vertical displacements or lateral shifts would produce systematic changes to the spin-label separations inconsistent with those observed. The switch from a primarily 4-helix bundle in H1 to a two-helix coiled-coil in H1-2 propagates directly across the bundle into the KCM, but this feature does not continue into the adaptation region. Rearrangements that propagate through the Gly hinge do not affect the helix separations across the bundle at all. A relatively modest change in hydrophobic packing seems a likely candidate for such a transition, but other plausible motions could involve helical rotation coupled to changes in helix separation, a scissors motion or a bend with the Gly hinge as the pivot point. In the PIR, increased dynamics are the dominant change measured by ESR, although changes in mean position could be masked by increased conformational breadth.

Changes in the dynamical state of separate KCM modules have been proposed in the context of a yin-yang model of receptor activation (14). This data was derived from the activity effects of Cys substitutions, disulfide cross-links and removal of hydrophobic side chains that stabilize the bundle core (socket positions) (14). Assessments of dynamics in the adaptation region show several engineered Cys pairs to have increased rates of cross-linking when local negative charge increases (17). Mutagenesis data on the HAMP domain also

suggests that destabilization of HAMP (or in fact its entire removal) produces a kinase-on state, whereas changes that stabilize hydrophobic packing at the base of AS2/AS2' produce a kinase-off state (15, 16, 40). It follows that HAMP dynamics likely influence KCM conformational properties. Despite agreement with these general ideas, our data reveal a more rigid PIR and dynamic HAMP in the kinase-on state, and the opposite for kinase-off. Evidence that the PIR becomes more dynamic in the kinase-on state largely comes from the "lock-on" effect of socket mutations that destabilize hydrophobic packing in this region (14). Notably, similar residue substitutions in the adaptation region stimulate CheR methylase activity and prevent kinase activation despite the receptors binding CheA/CheW (lock-off) (14). Despite the segregation of lock-on socket mutants to the PIR and lock-off socket mutants to the adaptation region, not all socket-altering substitutions comply with the yin-yang model (only 54% of mutants in the adaptation region and 62% in the PIR). Furthermore, although socket mutants in the receptor tip prevent deactivation by attractant, they only activate the kinase to normal levels (and sometimes less so). Thus, these substitutions may primarily short circuit deactivation signals that rely on proper transmission of packing changes within the bundle core. Likewise, disruption of packing interactions in the adaptation region by socket mutations may remove a stabilizing influence over the kinase-on conformation in the PIR. It is important to note that PIR dynamics in the ternary complex and the isolated receptors could differ, even with the former depending upon the latter. For example, in the kinase-off state, CheA and CheW may selectively stabilize a minor conformation of the PIR, only accessible because of increased dynamics (destabilization) enforced by HAMP. How the signaling particle responds to changes in receptor dynamics is the next important question. Recent data indicates that CheA activity depends on dynamics that involve both subtle coupling of domains through linkers (41) and large scale sequestration of the substrate (P1) domain (42).

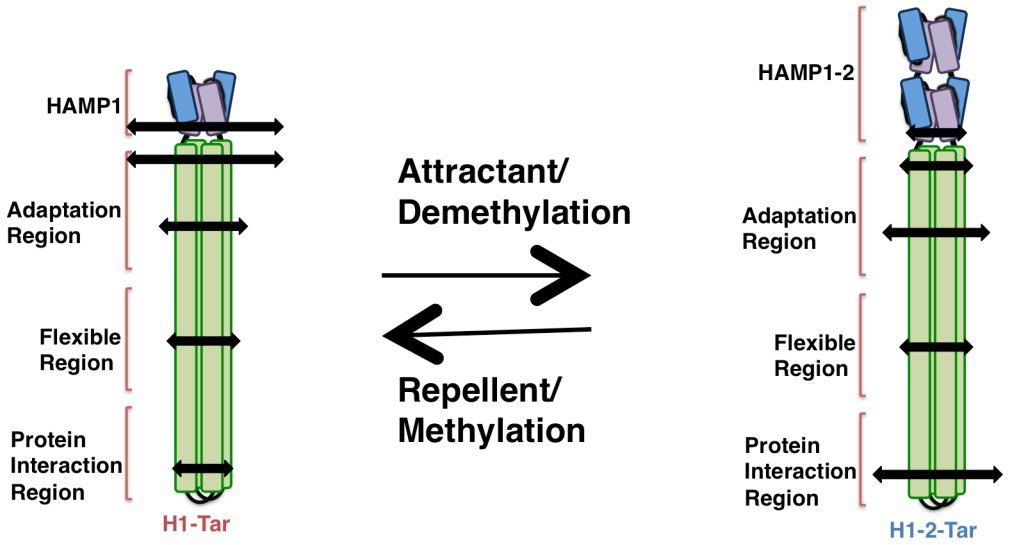

Figure 2-10: Dynamical properties of the HAMP-KCM. The HAMP and PIR show opposing dynamical properties depending on receptor activation state (length of arrow correlates with conformational breadth). Activating HAMP or increased modification produces a dynamic HAMP and static CheA/W-coupling tip. In contrast an inhibitory HAMP or decreased modification produce a conformationally stable HAMP, but dynamic CheA/W-coupling tip. Inversion of dynamics occurs at the Gly hinge, which does not change properties in any of the states tested.

CW-ESR spectra convolute the dynamic behavior of the spin-labeled side chain with that of the protein backbone (31, 32, 34). The inverse of the central line width (ΔH^{-1}) and overall spectral breadth (31) were employed to assess the mobility of TM1 in the ligand-free chemoreceptor Trg (43) and the C-terminal CheR-targeting peptide of Tar (44). Our CW-ESR data on the HAMP-KCM module indicates an equilibrium of two conformational states. In one state, the label is rigid on the ESR time scale (t_c > 10s of nanoseconds), and in the other, it is highly dynamic. These states may represent rigid helices that interact with the nitroxide and fluctuating chains that favor independent tumbling. For sites on

both the HAMP and KCM an increase in the rigid state fraction correlates with narrower PDS distributions. At higher temperature, the ESR time scale no longer discriminates the motional states as well, but preferences for the rigid component persist.

Many bacterial receptors and signal transduction proteins have a modular construction (7, 45). A general strategy for propagating conformational signals through such architectures may involve adjacent domains that influence the stability of each other via connections, which are often helical. For linear domain arrangements changes in hydrophobic packing and helix orientations can be effectively communicated through the connecting coiled-coils. At the extreme, these structural changes could involve near unfolding of the respective modules, relieving the influence of one domain over the other (4, 7). Altering output domain stability could impact enzymatic function or ability to engage partners. The inputs, such as ligand binding or change in cofactor state, alter stability of the binding domains to modulate their effects on downstream components. Signaling mechanisms based on competition for stability between adjacent domains can thereby allow different structural perturbations to achieve the same result. Conformational changes in a given context may well be specific, but they need not be unique. Thus competition between the dynamics of coupled protein modules may help explain the ease at which domain fusions have been elaborated into the many signaling architectures observed in nature.

2.4 Materials and Methods:

2.4.1 Cloning, Expression and Purification of Proteins:

H1-Tar and H1-2-Tar were initially cloned into pET28, as described previously (1). For binding experiments N-terminally S-tagged soluble effectors were generated by subcloning from pET28 into pET29c using NcoI and XhoI restriction sites. All the proteins were over-expressed in BL21(DE3) E. coli cells under 0.4 mM IPTG induction and for 16-20 hours at 25°C. Proteins were purified using Ni-NTA gravity column and subsequently on a Superdex 200 26-60 size exclusion

column with GF elution buffer: 20 mM Tris (pH 8.0), 150 mM NaCl, and 5-10% glycerol.

2.4.2 *In vivo* activity of H1-Tar and H1-2-Tar:

The data presented in Fig. 2-2A was originally reported in (25) under a procedure as follows: *E. coli* cells, devoid of all other receptors were transformed with the plasmid containing the gene of the effectors. Transformed cells were grown in terrific broth (TB), and were induced with 2 μM sodium salicylate for an hour. The cells were washed and kept in buffer containing 10 mM potassium phosphate, 0.1 mM EDTA (pH 7.0). Cell tumbling frequency was measured after 5 min, during when cells adapt, with dark-field microscopy.

2.4.3 *In vitro* CheY phospho-transfer assay:

Assay mixtures consisted of 20 μL 35% glycerol solution of 2 μM subunit concentrations of CheA and CheW each, 14.4 μM of effector subunit, 50 μM CheY and 2 μL of TKEM buffer [62.5 mM Tris, pH = 7.5, 625 mM KCl, 6.25 mM EDTA, and 125 mM $MgCl_2$] made up to volume with distilled water. The solution without CheY was incubated at 4°C for half an hour, and was further incubated for one and half an hour after CheY addition. After this time 5 μL of radio-active ATP solution [150 μL aqueous solution containing 12 μL of 12mM ATP, 1-7 μL of γ-^{32}P ATP (0.250 mCi, Perkin-Elmer) was added to the protein solution to initiate the phospho-transfer reaction. After 30 sec of exposure, the reaction was stopped with 25 μL of quenching buffer [3X LDS sample buffer, and 50 mM EDTA]. The sample was run on 4-20% Tris-Gly gel for 2h at 120 V to separate the components. After following the treatment described in (46), the gel was placed in the cassette, and the film was visualized in STORM phosphoimager after minimum of 24h of exposure. Densitometry with ImageJ software quantified the CheY band intensity after the background activity was removed by adjusting the brightness and contrast of the image.

2.4.4 Pull-down Experiments:

H1-Tar and H1-2-Tar with an N-terminal S-tag and a C-terminal His_6 tag were over-expressed from pET29c as described above. *E. coli* CheW and CheA were

expressed from pET28 following the same procedure and both carried N-terminal His_6 tags. After purification, the CheW His-tag was readily removed by thrombin digestion, but CheA His-tag removal was not complete, and hence pull-downs were performed with the S-tag. S-protein agarose (60 uL) was used to pull down S-tagged HAMP-Tar fusions and associated molecules from a 100 uL solution containing the three components in the subunit ratio of HAMP-Tar : EcCheA monomer : EcCheW monomer = 6 : 1 : 1 (195 uM of HAMP-Tar proteins, 65 uM of EcCheA and 70 uM of EcCheW). The S-agarose was washed twice with buffer containing 50 mM Tris (pH=8.0), 300 mM NaCl, 5% glycerol, and 62.5 mM KCl before boiling with 2x LDS sample buffer. The supernatant was then run on an SDS-PAGE gel, which was coomassie stained, destained with 25% ethanol and 10% acetic acid mixture and dried before quantification (ImageJ software). Molar ratios of bound CheA and CheW to effector were calculated from the intensities of the bands on SDS-PAGE gel measured with ImageJ software using the formula $((I_{CheA/CheW} - I_{background\ with\ same\ area}) / MW_{CheA/CheW}) / ((I_{HAMP1\text{-}Tar/HAMP1\text{-}2\text{-}Tar} - I_{background\ with\ same\ area}) / MW_{HAMP1\text{-}Tar/HAMP1\text{-}2\text{-}Tar})$.

2.4.5 Site Directed Spin Labeling:

Selected residues in the cysteinless HAMP-Tar proteins were mutated to cysteine using Quikchange PCR protocol (Stratagene). Cys-substituted effector molecules with N-terminally His_6 tag were overexpressed, as above. The proteins were bound to a Ni-NTA affinity column, and then reacted with cysteine-specific nitroxide MTSL spin label (Toronto Research Chemicals Inc.), on column for 3-4 hours at room temperature and subsequently for 4-6 hours at 4^oC before elution with {25 mM Hepes (pH=8.0), 250 mM Immidazole (pH=8.0), 500 mM NaCl, 10% Glycerol} buffer. Following elution, samples were subjected to size-exclusion chromatography (Superdex 200 26-60) for further purification and removal of unreacted MTSL contaminants. On-column spin labeling was adopted to minimize interdimer disulfide bond formation. Although cross-linking was limited by fast on-column exchange of reducing agents for spin-label, we could not avoid it entirely.

2.4.6 Pulsed Dipolar ESR Measurement:

As HAMP-Tar molecules are homodimers, one Cys substitution generates two spin labels per dimer. PDS was used to measure the distance distribution between these two spin labels, as previously described (25, 47). In brief, ~100 uM spin labeled dimer was prepared in GF buffer with 35% glycerol. The dipolar evolution at 17.35 GHz was measured on a home-built 2D FT-ESR instrument using 4-pulse double electron electron resonance (DEER) with a 16 ns pump pulse. The baseline of the time domain data was corrected with a linear polynomial function. DEER data was then converted to distance distribution between spin-pairs with Tikhonov regularization (48) followed by Maximum Entropy refinement (49). The distance distributions are normalized to unity for the ease of comparison.

2.4.7 CW ESR Data Collection and Analysis:

CW ESR data on the same spin-labeled samples were collected at three different temperatures, 4°C, 20°C, and 30°C on a Bruker Elexsys E500 EPR instrument at 9.4 GHz with 100 kHz modulation frequency and 1.6G modulation amplitude. Two components, one broad, representing a near rigid limit, and one sharper, representing faster motion, were observed at all temperatures, although their relative intensities did change. The fractions of these two components were determined by double integration of the experimental spectrum. A third minor component from a very small fraction of free MTSL does not affect estimates for the two major fractions. The spectra were analyzed using NLSL software (32) and its recent versions on the MATLAB platform. Initially, the spectral component corresponding to the broad signal (Fig. 2-8) was simulated and fit corresponding to very slow rotational diffusion with D_r ca. 0.8 - $1x10^7$ s^{-1}). This signal was then removed from the experimental spectrum by spectral subtraction, leaving just that of the more mobile component. Then the motional parameters for this component (Table 2-4) were estimated by NLSL simulations using the MOMD model (32).

2.5 Acknowledgements:

This work supported by NIH grant GM066775 to B.R.C. and P41GM103521 to J.H.F.

2.6 References:

1. Nygaard R*, et al.* (2013) The Dynamic Process of β 2-Adrenergic Receptor Activation. *Cell* 152(3):532-542.

2. Preininger AM, Meiler J, & Hamm HE (2013) Conformational Flexibility and Structural Dynamics in GPCR-Mediated G Protein Activation: A Perspective. *J. Mol. Biol.* 425(13):2288-2298.

3. Wiesner S*, et al.* (2006) A change in conformational dynamics underlies the activation of Eph receptor tyrosine kinases. *EMBO J.* 25:4686-4696.

4. Schultz JE & Natarajan J (2013) Regulated unfolding: a basic principle of intraprotein signaling in modular proteins. *Trends in Biochemical Sciences* 38(11):538-545.

5. Sourjik V & Wingreen NS (2012) Responding to chemical gradients: bacterial chemotaxis. *Curr. Opin. Cell Biol.* 24(2):262-268.

6. Hazelbauer GL, Falke JJ, & Parkinson JS (2008) Bacterial chemoreceptors: high-performance signaling in networked arrays. *Trends In Biochemical Sciences* 33(1):9-19.

7. Parkinson JS (2010) Signaling Mechanisms of HAMP Domains in Chemoreceptors and Sensor Kinases. *Annual Review of Microbiology* 64:101-122.

8. Falke JJ & Hazelbauer GL (2001) Transmembrane signaling in bacterial chemoreceptors. *Trends Biochem. Sci.* 26:257-265.

9. Dunten P & Koshland DE, Jr. (1991) Tuning the responsiveness of a sensory receptor via covalent modification. *J Biol Chem* 266(3):1491-1496.

10. Chervitz SA & Falke JJ (1996) Molecular mechanism of transmembrane signaling by the aspartate receptor: a model. *Proc Natl Acad Sci U S A* 93(6):2545-2550.

11. Hall BA, Armitage JP, & Sansom MSP (2011) Transmembrane Helix Dynamics of Bacterial Chemoreceptors Supports a Piston Model of Signalling. *Plos Computational Biology* 7(10).

12. Park H, Im W, & Seok C (2011) Transmembrane Signaling of Chemotaxis Receptor Tar: Insights from Molecular Dynamics Simulation Studies. *Biophys. J.* 100(12):2955-2963.

13. Kitanovic S, Ames P, & Parkinson JS (2011) Mutational Analysis of the Control Cable That Mediates Transmembrane Signaling in the Escherichia coli Serine Chemoreceptor. *J. Bacteriol.* 193(19):5062-5072.

14. Swain KE, Gonzalez MA, & Falke JJ (2009) Engineered Socket Study of Signaling through a Four-Helix Bundle: Evidence for a Yin-Yang Mechanism in the Kinase Control Module of the Aspartate Receptor. *Biochemistry* 48(39):9266-9277.

15. Zhou Q, Ames P, & Parkinson JS (2009) Mutational analyses of HAMP helices suggest a dynamic bundle model of input-output signalling in chemoreceptors. *Mol. Microbiol.* 73(5):801-814.

16. Zhou Q, Ames P, & Parkinson JS (2011) Biphasic control logic of HAMP domain signalling in the Escherichia coli serine chemoreceptor. *Mol. Microbiol.* 80(3):596-611.

17. Starrett DJ & Falke JJ (2005) Adaptation mechanism of the aspartate receptor: Electrostatics of the adaptation subdomain play a key role in modulating kinase activity. *Biochemistry* 44(5):1550-1560.

18. Coleman MD, Bass RB, Mehan RS, & Falke JJ (2005) Conserved glycine residues in the cytoplasmic domain of the aspartate receptor play

essential roles in kinase coupling and on-off switching. *Biochemistry* 44(21):7687-7695.

19. Swain KE & Falke JJ (2007) Structure of the conserved HAMP domain in an intact, membrane-bound chemoreceptor: A disulfide mapping study. *Biochemistry* 46:13684-13695.

20. Piasta KN, Ullimann CJ, Slivka PF, & Falke JJ (2013) Elucidating Receptor-CheA Kinase Contacts in the Membrane-Bound Chemosensory Array of Bacteria using Disulfide Mapping and TAM-IDS. *Biochemistry* 52(22):3866-3880.

21. Ferris HU*, et al.* (2011) The Mechanisms of HAMP-Mediated Signaling in Transmembrane Receptors. *Structure* 19(3):378-385.

22. Hulko M*, et al.* (2006) The HAMP domain structure implies helix rotation in transmembrane signaling. *Cell* 126(5):929-940.

23. Gushchin I, Gordeliy V, & Grudinin S (2013) Two Distinct States of the HAMP Domain from Sensory Rhodopsin Transducer Observed in Unbiased Molecular Dynamics Simulations. *Plos One* 8(7).

24. Ortega DR*, et al.* (2013) A phenylalanine rotameric switch for signal-state control in bacterial chemoreceptors. *Nat. Commun.* 4.

25. Airola MV*, et al.* (2013) HAMP domain conformers that propagate opposite signals in bacterial chemoreceptors. *PLoS Biol* 11(2):e1001479.

26. Airola MA, Watts KJ, & Crane BR (2010) Structure of concatenated HAMP domains provides a mechanism for signal transduction. *Structure* 18:436-448.

27. Briegel AL, X. Bilwes, A.M., Hughes, K.T., Jensen, G., Crane B.R. (2012) Bacterial chemoreceptor arrays are hexagonally packed trimers of

receptor dimers networked by rings of kinase and coupling proteins. *Proc. Natl. Acad. Sci. USA* 109:3766-3771.

28. Liu J*, et al.* (2012) Molecular architecture of chemoreceptor arrays revealed by cryoelectron tomography of Escherichia coli minicells. *Proc. Natl. Acad. Sci. U. S. A.* 109(23):E1481-E1488.

29. Borbat P & Freed J (2014) Pulse Dipolar Electron Spin Resonance: Distance Measurements. *Structural Information from Spin-Labels and Intrinsic Paramagnetic Centres in the Biosciences,* Structure and Bonding 152:1-82.

30. Barnes JP, Liang Z, McHaourab HS, Freed JH, & Hubbell WL (1999) A multifrequency electron spin resonance study of T4 lysozyme dynamics. *Biophys J* 76(6):3298-3306.

31. Liang Z, Lou Y, Freed JH, Columbus L, & Hubbell WL (2004) A Multifrequency Electron Spin Resonance Study of T4 Lysozyme Dynamics Using the Slowly Relaxing Local Structure Model. *The Journal of Physical Chemistry B* 108(45):17649-17659.

32. Budil DE, Lee S, Saxena S, & Freed JH (1996) Nonlinear-Least-Squares Analysis of Slow-Motion EPR Spectra in One and Two Dimensions Using a Modified Levenberg–Marquardt Algorithm. *Journal of Magnetic Resonance, Series A* 120(2):155-189.

33. Guo Z, Cascio D, Hideg K, & Hubbell WL (2008) Structural determinants of nitroxide motion in spin-labeled proteins: solvent-exposed sites in helix B of T4 lysozyme. *Protein science : a publication of the Protein Society* 17(2):228-239.

34. Zhang Z & Hendrickson WA (2010) Structural Characterization of the Predominant Family of Histidine Kinase Sensor Domains. *J. Mol. Biol.* 400(3):335-353.

35. Guo Z, Cascio D, Hideg K, Kalai T, & Hubbell WL (2007) Structural determinants of nitroxide motion in spin-labeled proteins: tertiary contact and solvent-inaccessible sites in helix G of T4 lysozyme. *Protein science : a publication of the Protein Society* 16(6):1069-1086.

36. Boldog T, Grimme S, Li MS, Sligar SG, & Hazelbauer GL (2006) Nanodiscs separate chemoreceptor oligomeric states and reveal their signaling properties. *Proc. Natl. Acad. Sci. U. S. A.* 103(31):11509-11514.

37. Bogonez E & Koshland DE (1985) Solubilization of a vectorial transmembrane receptor in functional form - aspartate receptor of chemotaxis. *Proc. Natl. Acad. Sci. U. S. A.* 82(15):4891-4895.

38. Borkovich KA, and Simon, M.I. (1991) Coupling of receptor function to phosphate-transfer reactions in bacterial chemotaxis. *Methods Enzymol.* 200:205-214.

39. Bornhorst JA & Falke JJ (2003) Quantitative analysis of aspartate receptor signaling complex reveals that the homogeneous two-state model is inadequate: Development of a heterogeneous two-state model. *J. Mol. Biol.* 326(5):1597-1614.

40. Ames P, Zhou Q, & Parkinson JS (2014) HAMP domain structural determinants for signalling and sensory adaptation in Tsr, the Escherichia coli serine chemoreceptor. *Mol. Microbiol.* 91(5):875-886.

41. Wang X*, et al.* (2014) The Linker between the Dimerization and Catalytic Domains of the CheA Histidine Kinase Propagates Changes in Structure and Dynamics That Are Important for Enzymatic Activity. *Biochemistry* 53(5):855-861.

42. Briegel A*, et al.* (2013) The mobility of two kinase domains in the Escherichia coli chemoreceptor array varies with signalling state. *Mol. Microbiol.* 89(5):831-841.

43. Barnakov A, Altenbach C, Barnakova L, Hubbell WL, & Hazelbauer GL (2002) Site-directed spin labeling of a bacterial chemoreceptor reveals a dynamic, loosely packed transmembrane domain. *Protein Sci.* 11(6):1472-1481.

44. Bartelli NL & Hazelbauer GL (2011) Direct evidence that the carboxyl-terminal sequence of a bacterial chemoreceptor is an unstructured linker and enzyme tether. *Protein Sci.* 20(11):1856-1866.

45. Uings IJ & Farrow SN (2000) Cell receptors and cell signalling. *Molecular Pathology* 53(6):295-299.

46. Sircar R, Greenswag AR, Bilwes AM, Gonzalez-Bonet G, Crane BR (2013) Structure and activity of the flagellar rotor protein FliY: A member of the CheC phosphatase family. J Biol Chem 288(19):13493–13502.

47. Bhatnagar J, Sircar R, Borbat PP, Freed JH, Crane BR (2012) Self-association of the histidine kinase CheA as studied by pulsed dipolar ESR spectroscopy. Biophys J 102(9): 2192–2201.

48. Chiang YW, Borbat PP, Freed JH (2005) The determination of pair distance distributions by pulsed ESR using Tikhonov regularization. J Magn Reson 172(2):279–295.

49. Chiang YW, Borbat PP, Freed JH (2005) Maximum entropy: A complement to Tikhonov regularization for determination of pair distance distributions by pulsed ESR. J Magn Reson 177(2):184–196.

Chapter Three

Bacterial Energy Sensor Aer Modulates Activity of the Chemotaxis Kinase CheA Based on Redox State of the Flavin Adenine Dinucleotide Cofactor

3.1 Introduction:

Bacteria search out conditions that provide sufficient energy to sustain homeostasis and fuel growth. In *E. coli*, so-called "Energy Taxis" (1–3), employs a sensory membrane protein, Aer, to monitor cellular internal energy state and convey that information to the chemotaxis system (4–6). Aer is related to bacterial chemoreceptors, also known methyl accepting chemotaxis proteins (MCP) that sense chemical ligands and ligand-binding proteins in the periplasmic space. However, unlike MCPs, the Aer sensor domains reside on the cytoplasmic side of the membrane and Aer lacks the methylation-based adaptation mechanism that provides negative feedback in chemosensing (7, 8). Homodimeric Aer (9) is composed of two N-terminal cytoplasmic PAS domains, a membrane anchor region composed of two transmembrane helices per subunit (TM1 and TM2) (10, 11), a cytoplasmic HAMP domain and a kinase control module (KCM) that binds and regulates the histidine kinase CheA. CheA, the coupling protein CheW, and MCPs form extended hexagonal arrays that are responsible for the signal gain and cooperative responses in chemotaxis. Within these arrays, a core complex composed of two receptor trimer-of-dimers, a dimeric CheA, and two CheW proteins comprise a minimal unit for signaling responses. The Aer PAS domains bind flavin adenine dinucleotide (FAD) (5, 7, 12) and are believed to receive redox signals from components of the electron transport chain (ETC) in the inner membrane (13).

Genetic and cellular experiments have determined that Aer mediates aerotaxis, but that this behavior does not involve direct reaction of Aer with O_2 (5, 14). Rather, Aer responds to the redox status of the ETC, which is in turn depends on

aerobic respiration (4, 5, 15). The prevailing model for Aer signaling has been derived largely from physiological data and involves the three redox states of FAD cofactor (13, 16, 17) (Fig. 3-1). In the absence of substrates to provide reducing equivalents, the FAD remains oxidized and Aer activates CheA autophosphorylation. CheA then transfers phosphate to the response regulator CheY, which binds to the flagellar motor and causes cell tumbling. When substrates and terminal electron acceptors are present, Aer inhibits CheA, causing smooth swimming. Under these conditions, Aer is assumed to be reduced to the semiquinone state by electrons in the ETC. With substrates present, but no terminal acceptors, cells tumble again, presumably due to complete reduction of FAD to hydroquinone state.

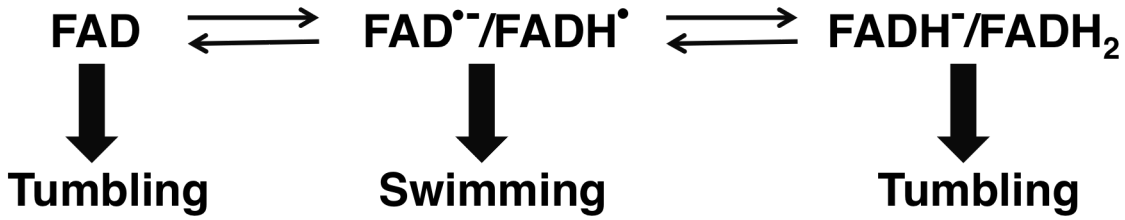

Figure 3-1: A hypothesis that connects FAD redox states in Aer with different modes of cellular movement.

There is currently no direct biochemical data correlating the redox state of the Aer PAS domain with kinase activity. Furthermore, although Aer clearly regulates CheA, it has not been determined if Aer forms similar core complexes with CheA and CheW as do other MCPs. Here we report the purification of *Escherichia coli* Aer and its incorporation into functional nanodiscs. We determine that the protein binds flavin as predicted, and that the cofactor undergoes chemical reduction to the anionic semiquinone. Aer assembles into the core complexes with CheA and CheW, in which it modulates CheA activity based on the redox state of FAD. No evidence is found for a stable hydroquinone form of the protein.

3.2 Results:

N-terminally His_6-tagged *E. coli* Aer was expressed in BL21(DE3) cells and purified in 0.1% n-dodecyl-β-D-maltopyranoside (DDM) using Co^{2+}-affinity chromatography (Fig. 3-2A). The purified Aer shows the signature UV-Vis spectrum of protein-bound FAD in the fully oxidized state (Fig. 3-2B). Previously, the Aer cofactor was confirmed to be FAD only after dissociation from the protein (5, 7). Aer binds approximately one FAD cofactor per subunit (Fig. 3-3A). Upon treatment with 10 mM dithionite in anaerobic conditions, the UV-Vis spectrum of the Aer-bound FAD converts to that of the single-electron reduced anionic semiquinone (ASQ) state. The ASQ reverts back to the fully oxidized cofactor on exposure to air (Fig. 3-2B) (18). The continuous wave electron spin resonance (cw-ESR) spectrum confirms the radical nature of the dithionite-reduced FAD, which becomes ESR silent upon reoxidation (Fig. 3-2C). Interestingly, prolonged anaerobic incubation of Aer with 16 mM dithionite does not yield the two-electron reduced hydroquinone (HQ) state. DDM is detrimental to CheA activity (Fig. 3-3B) and thus nanodisc incorporation was applied to stabilize Aer in the absence of detergent (19). Nanodiscs have served as an extremely useful method for reconstituting transmembrane MCPs in active forms (19), and the same holds true for Aer.

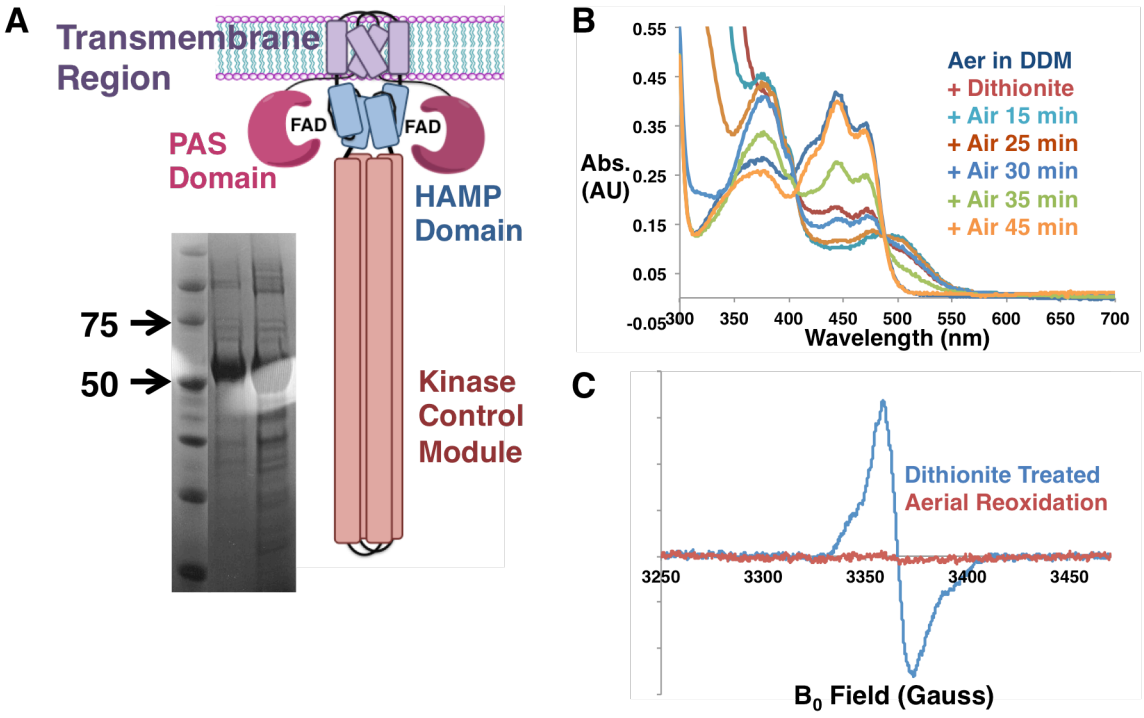

Figure 3-2: Purification and chemical reduction of EcAer. (A) The schematic of Aer displays the relative disposition of functional domains with respect to the membrane and each other. The inset shows an image of coomassie-stained SDS-PAGE gel. Lane 1: Markers with molecular weight of two bands; Lane 2 and 3: Elution from Co(II) column at various dilutions. (B) FAD in Aer dissolved in detergent is reduced with 10 mM sodium dithionite and UV-Vis spectra are collected at different times. (B) cw-ESR spectra of dithionite-reduced and aerially reoxidized FAD in Aer are shown.

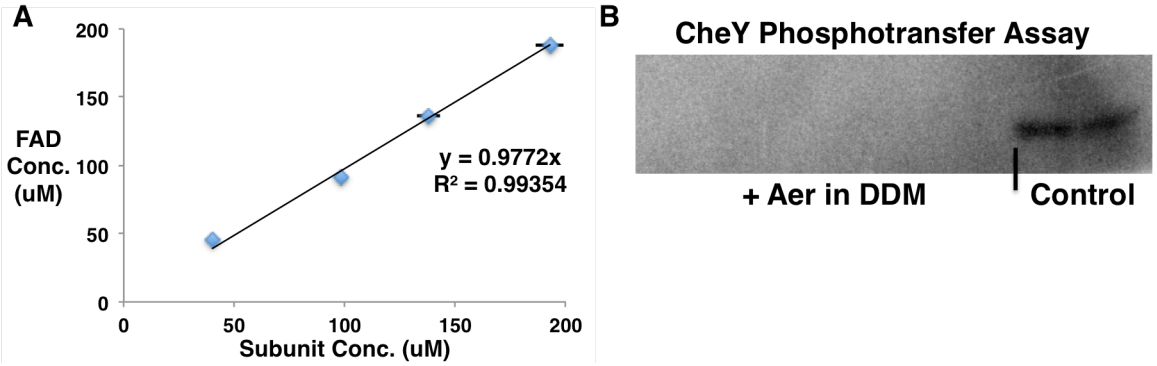

Figure 3-3: Quantification of FAD binding to Aer and the effect of detergent on CheA activity. (A) Independently measured Aer subunit concentrations and FAD concentrations of serially diluted samples are plotted against each other. The concentrations of FAD are calculated from the absorbance at 445 nm with the extinction coefficient of free FAD (ε_{445} = 11,300 M^{-1} cm^{-1}) (20) and the subunit concentrations are measured using the Bradford assay. (B) CheY phosphotransfer assay confirms DDM damage of CheA activity.

Aer was incorporated into nanodiscs assembled with *E. coli* polar lipids and the membrane scaffold protein, MSP1E3D1. As in detergent, Aer in nanodiscs can be reversibly reduced to the ASQ state upon dithionite treatment (Fig. 3-4A, 3-4B). Ternary signaling complexes of the major *E. coli* MCPs Tar (aspartate receptor) and Tsr (serine receptor) (19, 21) with CheA and CheW require a trimer of receptor dimers to fully activate CheA. To verify if Aer also functions through

ternary signaling complexes we produce two nanodisc preparations with the intention to vary the number of Aer dimers per nanodisc. One preparation is produced with molar ratio of Aer to MSP1E3D1 of 1:5 and the other with the ratio of 1:1. Previously by using these ratios of Tar to MSP1E3D1, on average one and more than two Tar dimers, respectively, were successfully incorporated into each nanodisc (19, 22, 23). Hence we presume that 1:5 and 1:1 preparations most likely contain on average one and more than two Aer dimers, respectively. The ability of CheA to catalyze phosphotransfer to CheY was substantially higher with 1:1 preparation compared to 1:5 preparation (Fig. 3-4C). Notably, insertion of Aer into the symmetric disks could be with one of two polarities, and three dimers pointing in the same direction is needed to fully activate the kinase. We also note that the lesser CheA activition observed in the ~1 dimer / disk sample may owe to either reduced activation by one dimer, or activation by a small statistically weighted subset of samples of three parallel dimers per disk. Upon chemical reduction of Aer to the ASQ, CheA activity is inhibited (Fig. 3-4D). Reoxidation by air then partially recovers the activity. A control experiment shows no loss of CheA activity upon only dithionite addition (Fig. 3-5) verifying that the CheA inhibition is due to reduction of Aer to the ASQ state. Thus, Aer in its oxidized FAD form activates CheA and would therefore cause cell tumbling. Reduction of Aer to the ASQ reversibly inhibits kinase activity and would cause smooth swimming. Even the low-potential reductant dithionite was unable to produce the hydroquinone state, although dithionite reduces the FAD cofactor in *Azotobacter vinelandii* NifL, a homolog of the Aer PAS domain, to fully reduced hydroquinone state (20). Further reduction of Aer may be limited by its preference to form the anionic instead of the neutral seminquinone. Reduction to the hydroquinone requires additional proton transfer, which may be kinetically disfavored under these conditions. If oxygen were to react directly with Aer it would not be expected to produce a smooth swimming response, because this behavior requires reduced FAD, which O_2 destabilizes. Thus, the activity data supports the assertion that oxygen facilitates reduction of the Aer FAD by acting as a terminal acceptor to the ETC.

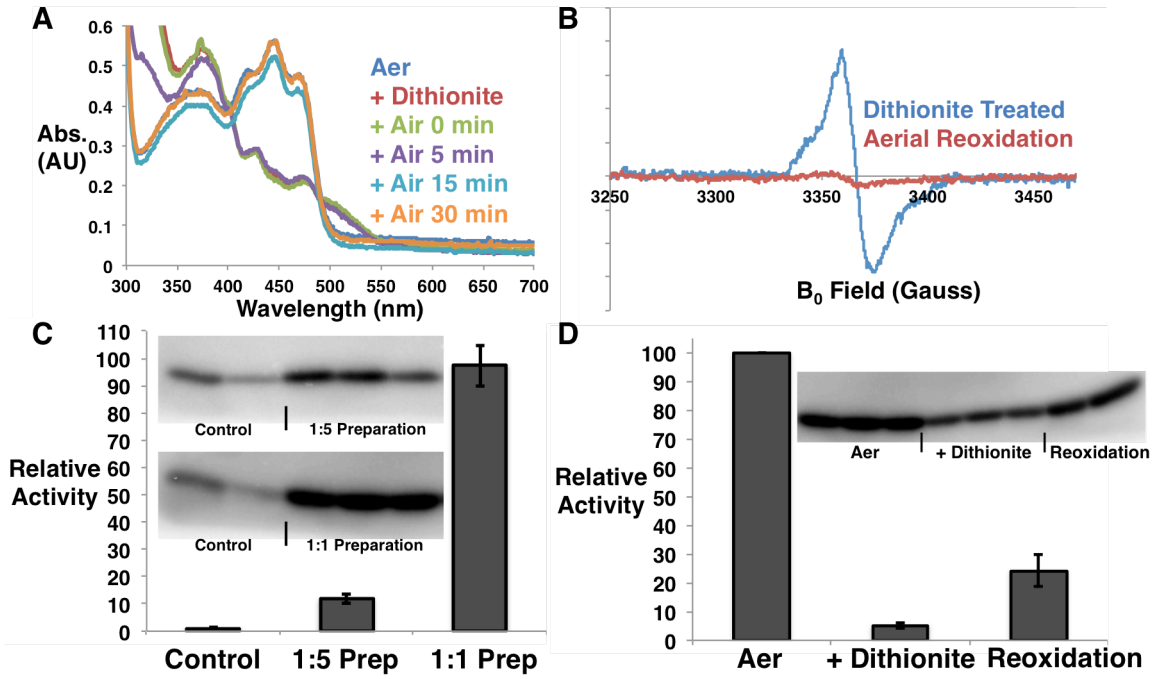

Figure 3-4: Characterization and functional implication of various redox states of FAD in Aer. UV-Vis spectra (A) and cw-ESR spectra (B) at different times during dithionite reduction and ambient reoxidation of FAD in Aer incorporated in nanodiscs are coded in color relative to the legend. (C) CheA activities with 1:5 and 1:1 preparations that presumably contain ~one and ~three Aer dimers per nanodisc are compared. The activities are measured relative to the control sample, which contains only CheA, CheW, and CheY. Inset shows the image of the gels from the CheY phosphotransfer experiments. (D) Modulation of CheA activity by fully oxidized and ASQ states of FAD along with recovery of activity upon reoxidation with the inset showing representative band intensities.

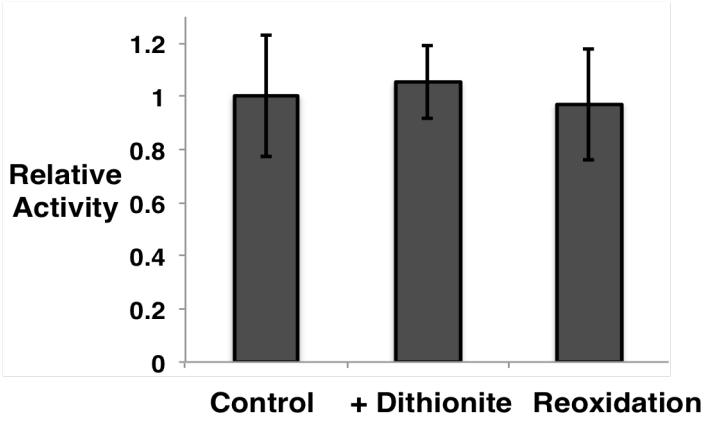

Figure 3-5: Control experiment showing no interference of dithionite on CheA activity. CheY phosphotransfer assay verified no loss of kinase activity by dithionite addition and ambient reoxidation. Control represents sample containing CheA, CheW, and CheY proteins.

3.3 Discussion:

Configurations of cofactors modulate the activity of proteins and organismal responses to environmental stimuli. For example, the bilin cofactor in phytochromes guides seed germination, timing of flowering, etc. in response to near infrared light (24, 25), the FMN cofactor in phototropin governs blue light-mediated phototropism in plants (26, 27), the FAD cofactor in bacterial NifL regulates nitrogen fixation process based on oxygen availability (20). Here we provide experimental evidence linking redox states of FAD cofactor with the regulation of bacterial energy taxis by Aer protein.

Oxidation of nutrients supplies electron equivalents to the ETC to which the Aer PAS domain directly responds. Components of ETC and thus FAD in Aer will be oxidized in absence of nutrients, whereas in presence of both nutrients and terminal electron acceptor FAD undergoes single electron reduction due to continuous electron flow through ETC. Thus our data provide direct evidence for how these changes in redox state regulate bacterial movement away from an environment deficient in nutrients.

Conversion to the two-electron reduced hydroquinone state of FAD in Aer has been postulated to explain a cellular tumbling response upon removal of terminal electron acceptors. However, even treatment with low-potential dithionite could not generate such a state in Aer. Attempts will be made to reduce Aer to the hydroquinone by other means and we will investigate whether other partners are required to explain the cellular tumbling response upon deoxygenation or removal of other terminal electron acceptors.

3.4 Methods:

3.4.1 *E. coli* Aer Expression and Purification:

BL21(DE3) cells were transformed with pET28 vector containing N-terminally His_6-tagged *E. coli* Aer, plated on kanamycin-added LB-agar plate, and incubated at 37 °C overnight. A single colony was added to autoclaved and kanamycin-mixed LB media for overnight growth under 200 rpm shake at 37 °C. 1 L of autoclaved and antibiotic added TB media was inoculated with 20 ml of the overnight. The cells were then grown at 37 °C until OD_{600} reaches ~ 0.3. The temperature was turned down to 16 °C while cell growth continues until OD_{600} = 0.6 - 0.8 at which point the expression was induced by adding IPTG. Cells were harvested after overnight expression and stored at -80 °C.

The cells were resuspended in KCl extraction buffer {50 mM Tris pH 8.0, 500 mM KCl, and 10% Glycerol}, sonicated for 5 - 6 min, and centrifuged at 10,000 rpm for 30 min to obtain the membrane fractions in the pellet, low-spin pellet (LSP), which was again resuspended in KCl extraction buffer added with 1 mM PMSF and 1% DDM. The resuspended LSP was first sonicated at low power to ensure fine resuspension and then at high power for 2 min before rocking at 4 °C for 5 hrs. and centrifuging at 22,000 rpm for 1 hr. The supernatant was added with 0.1 mg/ml FAD and was incubated with Co(II) resins in falcon tubes overnight. The next morning the resins were packed at the bottom of the tubes by centrifugation, the supernatant was removed, and the resins were resuspended in buffer {50 mM Tris pH 8.0, 300 mM NaCl, and 10% Glycerol}. DDM concentration was maintained at 0.1% this step onwards. In similar way, the resins were washed several times with wash buffer {25 mM Tris pH 8.0, 150 mM NaCl, and 10% Glycerol} containing 0.1% DDM and 0.1 mg/ml FAD. Then the resins were transferred to a column, washed with more wash buffer added with 0.1% DDM and 0.1 mg/ml FAD, then with buffer without FAD, and finally Aer protein was eluted from the resins with elution buffer {25 mM Tris pH 8.0, 150 mM NaCl, 10% Glycerol, 0.1% DDM, and 200 mM Imidazole pH 8.0}. UV-Vis spectrum was acquired to ensure that Aer contains FAD.

3.4.2 Aer incorporation into nanodisc:

Detergent purified Aer was incorporated into lipidic nanodiscs following the protocols described in various articles (22, 28, 29). Briefly, chloroform was evaporated from *E. coli* polar lipid stock by blowing argon and further by keeping in vacuum chamber overnight. The lipid was then dissolved in sodium cholate in the form of vesicles by sonication and stored at -80 °C. Membrane scaffold protein His_6-MSP1E3D1 was purified from BL21(DE3) as described elsewhere (28, 29). Aer, MSP1E3D1, and lipid were mixed in the ratio of Aer subunit: MSP1E3D1 subunit: lipid = 1: 1: 120 or 1: 5: 750 to incorporate approximately one and three Aer dimers per nanodisc, respectively. 22.22 mM sodium cholate, 5% glycerol, and 0.1 mg/ml FAD were maintained into the reaction mixture to ensure solubility and stability. The mixture was rocked at 4 °C for 30 min before pre-hydrated biobeads of volume of 2/3 of the mixture were added and further incubated at 4 °C for 1.5 hrs. The mixture was then centrifuged at 13,000 rpm for 12 min and the supernatant was further purified either through size exclusion chromatography or in desalting column to separate the nanodiscs from free FAD and excess lipids.

3.4.3 Sodium dithionite reduction of Aer and aerial reoxidation:

10 mM sodium dithionite was added to Aer from a stock of 100 mM prepared in 1 M tris, pH 8.0 in the glovebox and UV-Vis spectra were recorded with a cuvette of 0.2 cm path-length sealed with parafilm. To follow aerial reoxidation, the parafilm seal was opened, the cuvette was stored in 4 °C refrigerator, and at different times spectra were recorded.

3.4.4 cw-ESR spectra collection:

cw-ESR spectra were collected at 4 °C on Bruker Elexsys E500 EPR instrument at 9.4 GHz with 100 kHz modulation frequency and 1.5 or 2 G modulation amplitude. Dithionite reduced spectra of Aer were contaminated with dithionite features, which were subtracted in matlab.

3.4.5 CheY phosphotransfer assay:

The procedure followed for CheY phosphotransfer assay is very similar to as described elsewhere (30). Briefly, samples containing CheA subunit: CheW: Aer subunit: CheY = 2 μM: 3 μM: 15 μM: 50 μM were produced and treated with no (fully oxidized state), 16 mM (ASQ state), or 8 mM (for recovery) dithionite from a stock of 100 mM in 1 M Tris, pH 8.0. To follow stimulation by ASQ state, dithionite was added just prior to ATP addition, whereas for the recovery experiment the samples were incubated open to air at 4 °C for 2 hrs. after dithionite addition and prior to ATP exposure.

3.5 References:

1. Taylor BL (1983) How do bacteria find the optimal concentration of oxygen? *Trends Biochem Sci* 8(12):438–441.

2. Zhulin I, Johnson M, Taylor B (1997) How Do Bacteria Avoid High Oxygen Concentrations? *Biosci Rep* 17(3):335–342.

3. Taylor BL, Zhulin IB, Johnson MS (1999) Aerotaxis and other energy-sensing behavior in bacteria. *Annu Rev Microbiol* 53:103–128.

4. Rebbapragada A, et al. (1997) The Aer protein and the serine chemoreceptor Tsr independently sense intracellular energy levels and transduce oxygen, redox, and energy signals for Escherichia coli behavior. *Proc Natl Acad Sci* 94(20):10541–10546.

5. Bibikov SI, Biran R, Rudd KE, Parkinson JS (1997) A signal transducer for aerotaxis in Escherichia coli. *J Bacteriol* 179(12):4075–4079.

6. Watts KJ, Johnson MS, Taylor BL (2008) Structure-function relationships in the HAMP and proximal signaling domains of the aerotaxis receptor Aer. *J Bacteriol* 190(6):2118–2127.

7. Bibikov SI, Barnes LA, Gitin Y, Parkinson JS (2000) Domain organization and flavin adenine dinucleotide-binding determinants in the aerotaxis signal transducer Aer of Escherichia coli. *Proc Natl Acad Sci U S A* 97(11):5830–5835.

8. Bibikov SI, Miller AC, Gosink KK, Parkinson JS (2004) Methylation-independent aerotaxis mediated by the Escherichia coli Aer protein. *J Bacteriol* 186(12):3730–3737.

9. Ma Q, Roy F, Herrmann S, Taylor BL, Johnson MS (2004) The Aer protein of Escherichia coli forms a homodimer independent of the signaling domain and flavin adenine dinucleotide binding. *J Bacteriol* 186(21):7456–7459.

10. Amin DN, Taylor BL, Johnson MS (2006) Topology and boundaries of the aerotaxis receptor Aer in the membrane of Escherichia coli. *J Bacteriol* 188(3):894–901.

11. Amin DN, Taylor BL, Johnson MS (2007) Organization of the Aerotaxis Receptor Aer in the Membrane of Escherichia coli. *J Bacteriol* 189(20):7206–7212.

12. Ma Q, Johnson MS, Taylor BL (2005) Genetic analysis of the HAMP domain of the Aer aerotaxis sensor localizes flavin adenine dinucleotide-binding determinants to the AS-2 helix. *J Bacteriol* 187(1):193–201.

13. Repik A, et al. (2000) PAS domain residues involved in signal transduction by the Aer redox sensor of Escherichia coli. *Mol Microbiol* 36(4):806–816.

14. Laszlo DJ, Fandrich BL, Sivaram A, Chance B, Taylor BL (1984) Cytochrome o as a terminal oxidase and receptor for aerotaxis in Salmonella typhimurium. *J Bacteriol* 159(2):663–667.

15. Zhulin IB, Rowsell EH, Johnson MS, Taylor BL (1997) Glycerol elicits energy taxis of Escherichia coli and Salmonella typhimurium. *J Bacteriol* 179(10):3196–3201.

16. Taylor BL, Rebbapragada A, Johnson MS (2001) The FAD-PAS domain as a sensor for behavioral responses in Escherichia coli. *Antioxid Redox Signal* 3(5):867–879.

17. Taylor BL (2007) Aer on the inside looking out: paradigm for a PAS-HAMP role in sensing oxygen, redox and energy. *Mol Microbiol* 65(6):1415–1424.

18. Liu B, Liu H, Zhong D, Lin C (2010) Searching for a photocycle of the cryptochrome photoreceptors. *Curr Opin Plant Biol* 13(5):578–586.

19. Boldog T, Grimme S, Li M, Sligar SG, Hazelbauer GL (2006) Nanodiscs separate chemoreceptor oligomeric states and reveal their signaling properties. *Proc Natl Acad Sci* 103(31):11509–11514.

20. Hill S, Austin S, Eydmann T, Jones T, Dixon R (1996) Azotobacter vinelandii NIFL is a flavoprotein that modulates transcriptional activation of nitrogen-fixation genes via a redox-sensitive switch. *Proc Natl Acad Sci U S A* 93(5):2143–2148.

21. Briegel A, et al. (2012) Bacterial chemoreceptor arrays are hexagonally packed trimers of receptor dimers networked by rings of kinase and coupling proteins. *Proc Natl Acad Sci U S A* 109(10):3766–3771.

22. Boldog T, Li M, Hazelbauer GL (2007) Using Nanodiscs to create water-soluble transmembrane chemoreceptors inserted in lipid bilayers. *Methods Enzymol* 423:317–335.

23. Bartelli NL, Hazelbauer GL (2015) Differential backbone dynamics of companion helices in the extended helical coiled-coil domain of a bacterial chemoreceptor. *Protein Sci Publ Protein Soc* 24(11):1764–1776.

24. Casal JJ, Sánchez RA (1998) Phytochromes and seed germination. *Seed Sci Res* 8(03):317–329.

25. Burgie ES, Vierstra RD (2014) Phytochromes: an atomic perspective on photoactivation and signaling. *Plant Cell* 26(12):4568–4583.

26. Briggs WR (2014) Phototropism: some history, some puzzles, and a look ahead. *Plant Physiol* 164(1):13–23.

27. Liscum E, et al. (2014) Phototropism: growing towards an understanding of plant movement. *Plant Cell* 26(1):38–55.

28. Ritchie TK, et al. (2009) Chapter 11 - Reconstitution of membrane proteins in phospholipid bilayer nanodiscs. *Methods Enzymol* 464:211–231.

29. Karasawa A, et al. (2013) Physicochemical factors controlling the activity and energy coupling of an ionic strength-gated ATP-binding cassette (ABC) transporter. *J Biol Chem* 288(41):29862–29871.

30. Samanta D, Borbat PP, Dzikovski B, Freed JH, Crane BR (2015) Bacterial chemoreceptor dynamics correlate with activity state and are coupled over long distances. *Proc Natl Acad Sci U S A* 112(8):2455–2460.

Chapter Four

Means for the Propagation of Allosteric Communications

4.1 Introduction:

Allostery is the coupling between two distant sites in a protein or protein complex whereby changes in one site, called the regulatory site, alter the activity at a distant part, called the active site or the output domain (1–6). J. P. Changeux first observed allostery while studying L-isoleucine inhibition of L-threonine deaminase, which deaminates L-threonine to form α-ketobutyric acid (7, 8). Since then, the allosteric regulation has been realized to be so prevalent in modulating protein activity and thereby controlling cellular processes that it appears to be the second secret of life, genetic code being the first (9–11). Binding of small molecules, a partner or changes in the microenvironment modifies either or both the structure and dynamics of the regulatory site. Protein backbone and the side chains relay this effect to the active site to alter the protein activity either by adjusting the population of the active state or by varying the structure and/or dynamics of the active site to make it competent for the desired outcome.

Although phenomenological theories (MWC model and KNF model) exist to describe the allostery and cooperativity (12, 13), the mechanism of the transmission of the effect is unique to the system under study. Despite the uniqueness, the relay mechanism can be categorized under two topics: conformational changes, and dynamical changes of the regions intervening the two sites (Fig. 4-1). In many proteins, parts of the intervening regions may undergo changes in only structure, parts in only dynamics, and other parts in both structure and dynamics. Generally speaking, the spectrum of changes in the intervening regions can be explained by combination of these two extreme mechanisms. It is also important to note that our knowledge about the mechanism of allosteric propagation depends on the spectroscopic/structural method applied to probe the process. While X-ray crystallography (14–16), small angle X-ray scattering (SAXS) (17, 18), and cryo-electron microscopy (Cryo-EM)

(19, 20) can detect subtle structural reorganizations, they are not suitable for directly probing dynamical changes in a system. On the other hand, more recent developments, for example nuclear magnetic resonance (NMR) (21, 22), single molecule fluorescence resonance energy transfer (smFRET) (23, 24), and pulse-dipolar electron spin resonance (PDS-ESR) (25–27) techniques are well suited for dynamics measurements.

Conformational changes alter the enthalpy of the system (ΔH) whereas dynamics determine the entropy, and thus both the mechanisms will relate to the changes in the free energy, ΔG, according to the equation $\Delta G = \Delta H - T\,\Delta S$, where T designates the absolute temperature. To note, since various spectroscopic and/or structural methods probe structural and/or dynamical changes, our knowledge on the mechanism of allosteric propagation depends on the approach employed to characterize the process, and an accurate description can be obtained only by combining data from diverse experiments. In this review we will look into few examples of each of the two categories to explain the general principle of the two mechanisms.

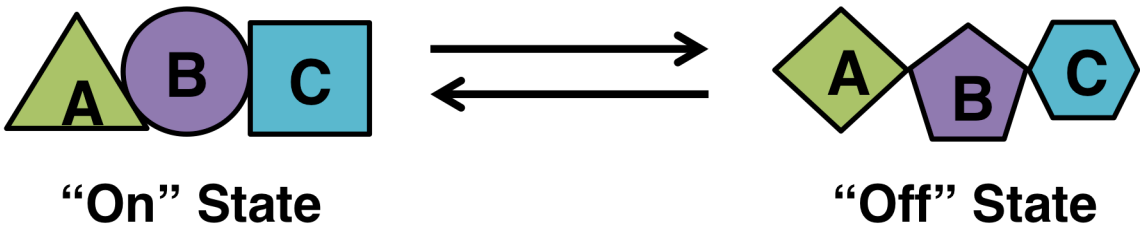

Figure 4-1: Different states of the motifs/domains intervening the allosterically coupled sites can be characterized by differences in structure and/or dynamics. Different states of three intervening motifs/domains in the two functional states of the proteins are depicted in different shapes. The two states of each motif/domain can be characterized either by a change in conformation or in dynamics.

4.2 Allosteric transmission involving mainly conformational changes in the intervening regions:

Even though the theories on allosteric effect existed at the time, determination of atomic scale structure of deoxyhemoglobin and methemoglobin by M. F. Perutz around the year of 1970 ushered in the era of the structural view of allosteric propagation, known as the “classical view”, where the allostery passes on by a series of conformational changes in the intervening regions (1, 14, 15, 28, 29). In the case of hemoglobin, oxygen binding to one or two subunits in the deoxy form of the tetrameric protein pulls the iron atoms to the porphyrin plane. The iron atom relocation draws the F helix towards H helix and the consequent steric strain releases the tyrosine side chain from the pocket between the two helices. Subsequent disruption of the salt bridges between the C termini results in the rotation of the subunits with respect to each other. These series of changes ultimately pre-organize the other oxygen binding centers to the binding-compatible structure.

Propagation of the interaction between different sites in a macromolecule via structural rearrangements of the intervening regions is vividly described in *E. coli* aspartate transcarbamoylase (ATCase), an exemplary system to describe the inhibition of metabolic enzymes by the end products of the metabolic pathways (30–32). ATCase catalyzes carbamoylation of the amino group in the substrate, L-aspartate by carbamoyl phosphate (CP) in pyrimidine neucleotide biosynthesis pathway. The carbamoyl transfer reaction is allosterically regulated by the activator ATP and the inhibitor CTP. ATCases are composed of two catalytic trimers and three regulatory dimers with D3 symmetry or with C3 symmetry when bound to CTP. The catalytic and regulatory chains are composed of two domains each: N-terminal and C-terminal domains. A number of crystal structures of ATCases bound with substrate, substrate analogs, CP, CTP, and combination thereof, along with structures of unliganded ATCases have elucidated the structural rearrangements during the transition from the inactive T state to the active R state. The structures of ATCase bound with bisubstrate analog, N-phosphonacetyl-L-aspartate (PALA) has been particularly enlightening to

uncover the conformational changes. An elongation of 11 Å along the molecular three-fold axis, a 12° rotation of one catalytic trimers with respect to the other, and a 15° rotation of each of the regulatory dimers along the two-fold axes characterize the quaternary changes associated with the transition from the T to the R state. ATCases bind CP before L-aspartate. Binding of CP in the T state reorganizes the loops containing the residues 76-85 and 225-245 in order to create a pocket with appropriate electrostatic environment for binding L-aspartate. Thus bound L-aspartate rearranges 225-245 loop so as to correctly position the amino group of L-aspartate within 2.8 Å of the carbonyl carbon of CP for nucleophilic attack. The rearrangement of the residues 225-245 entails the previously mentioned quaternary changes and a concomitant closure of the two domains of the catalytic chains by 6.8°. These series of changes destabilizes the T state and help the transition to the R state. The ATP or CTP binding in the N-terminal domain of the regulatory chains almost 60 Å away from the L-aspartate binding site repositions R229 as the mean to manifest the allosteric effect. ATP binding moves R229 towards the L-aspartate binding pocket and increases the binding affinity by enhancing the electrostatic interaction, whereas R229 moves away from the pocket upon CTP binding and thus causing the negative allostery.

Subtle conformational changes are also in effect to convey the allostery in CheY, a response regulator in bacterial chemotaxis (33–38). Phosphorylation of Asp57 (in *E. coli*) by the kinase CheA allows CheY to strongly bind the flagellar motor protein FliM causing clockwise rotation of flagella, which rotates in the counter-clockwise direction otherwise (39, 40). The enhancement in the binding affinity upon phosphorylation arises because Tyr106, a residue more than 9.5 Å away from the phosphorylation site, populates more in a buried conformation compared to a solvent exposed state, which is more populated in unphosphorylated form of CheY. The change in the population bias in turn results from the displacement of Thr87 towards the phosphorylation site and the conformational changes of the β4-α4 loop (Ala88-Lys91) by a root-mean-square deviation of 3.6 Å (for all non-hydrogen atoms).

Conformational rearrangements in the intervening regions carry the allosteric coupling also in photosensor VVD involved in the circadian rhythm in *Neurospora crassa* (41–44). VVD dimerizes and becomes active in the presence of blue light from inactive monomeric state in the dark. Upon photoactivation the isoalloxazine ring in the FAD moiety forms adduct with the Cys108 (45–47). The adduct formation protonates the N5 of FAD resulting in a modification in the H-bonding network in the PAS domain. The modified H-bonding network leads to a conformational change in the hinge region that repositions the N-terminal helix, called N-cap, and consequently the N-terminus, the N-terminal latch, is released from the core of the PAS domain. Thus, the remodeling of the domain releases the N-terminal latch along with creating a pocket under the hinge region to accept the latch from another subunit and thereby causing dimerization.

In the above examples subtle changes in the regulatory sites alter mainly the enthalpic landscape of the intervening regions in order to reorganize the active sites.

4.3 Allosteric transmission mainly involving dynamical changes in the intervening regions:

Dynamics are intimately linked with the protein activity (48–51) as shown by the loss of activity below 220 K. Cooper and Dryden in their seminal article published in 1984 correctly recognized the influence of dynamical changes in the allosteric communication, which since then has garnered tremendous appreciation (52). Association of dynamics with the allostery has been observed in both engineered and naturally occurring proteins. Two protein systems were engineered by fusing ribonuclease Barnase from *Bacillus amyloliquefaciens* with either human Ubiquitin or DNA binding domain of GCN4 in a way that only one domain in these two-domain chimeras can stay folded at any given time (53, 54). External factors such as temperature and ligand binding, decide which of the two domains would be folded and active. This regulated folding as a means to propagate the allostery is also seen in naturally occurring proteins such as pH-sensing adenylyl cylcase RV1264 from *Mycobacterium tuberculosis* (55, 56). The protein has three

distinct segments: the N-terminal regulatory domain (amino acid residues 14-191), a flexible linker region (residues 192-213), and the C-terminal catalytic domain (residues 214-377). The linker region undergoes regulated unfolding upon pH-activation: it assumes an α-helical structure (residues 192-206) and assists the regulatory domain to impose inhibitory constraint on the catalytic core at high pH, whereas at low pH the region partially unfolds to relieve the catalytic domain from the constraint imposed upon by the other domain and thus activates the protein. Another segment called α1 switch helix (residues 226-231) also experiences coil-to-helix transition upon pH-activation. Even more dramatic changes in the intervening regions occur in bacteriophytochromes from *D. radiodurans* upon light exposure (57). Isomerization of the biliverdin chromophore induced by red light unfolds the beta hairpin structure in the tongue region (residues 446-477), which connects the PHY domain with the photosensory core, while at the same time folds the adjacent residues into α helix. These restructuring of the tongue region eventually separates the two PHY domains in the dimeric protein apart, as a means to control the downstream signaling.

The homodimer of the cAMP binding domains in CAP protein epitomizes the entropic contributions to the allostery ensued from dynamics changes in the ps-ns time scale (21, 58). Two cAMPs bind the two subunits in the homodimer more than 24 Å apart and with negative cooperativity. Exquisite NMR studies have disclosed that while binding of the first ligand increases μs-ms dynamics and minimally affects the structure of the other binding motif, binding of the second ligand extensively dampens ps-ns dynamics in the dimer. The stiffening of the fast scale dynamics upon second ligand binding gives rise to a strong entropic penalty causing the negative cooperativity.

Dynamical changes along with conformational changes also play roles in signal transduction by transmembrane receptors including bacterial chemoreceptors and beta-2 adrenergic receptor (β_2AR), a prototypical G-protein-coupled receptor (GPCR). In *E. coli*, the bacterial chemoreceptors detect chemicals in the

periplasm, relay the information inside the cells, and modulate the activity of the kinase bound at the cytoplasmic tip, almost 380 Å away from the ligand binding pocket. Upon ligand binding, one of the helices, α4, in the periplasmic domain and the second transmembrane helix (TM2) undergo piston displacement perpendicular to the membrane plane (59–61). This conformational change propagates in the cytoplasmic domain by altering the local dynamics. The membrane proximal HAMP domain, a parallel four helix bundle, arguably changes its packing stability and experience an order-disorder transition (62–64). The membrane distal kinase control module (KCM), antiparallel four helical bundle, faces even more dramatic variation in dynamics (65, 66, 27). The HAMP proximal and distal part of the KCM experience polarized change in mobility: if one part becomes more dynamic the other stiffens and vice versa, whereas the intervening segment acts as a pivot point and stays similarly dynamic during the signal transmission. This polarized change in dynamics is potentially a versatile mechanism for allosteric communication in modular proteins. These results show that conformational changes (ΔH) in TM2 upon ligand binding manifests in the change in entropy (ΔS) in other segments, namely in HAMP domain and KCM, thereby revealing the interchangeability of enthalpic and entropic contribution to the change in free energy along the propagation of allosteric communication.

Along the line of bacterial chemoreceptors, in β_2AR also, binding of agonist, inverse agonist, and G-protein mimetic nanobody differentially modulate the dynamics in the transmembrane core and the cytoplasmic regions as a means to regulate various signaling pathways (67, 22). Relaxation dispersion NMR measurements clearly show that agonist binding enhances dynamics in the cytoplasmic interface, which is stabilized only after binding to G-proteins. This increased dynamics in the cytoplasmic interface upon agonist binding is postulated to favor binding to different G-proteins and even non-G proteins and thereby to regulate various intracellular signaling.

4.4 References:

1. Perutz MF, Wilkinson AJ, Paoli M, Dodson GG (1998) The stereochemical mechanism of the cooperative effects in hemoglobin revisited. *Annu Rev Biophys Biomol Struct* 27. doi:10.1146/annurev.biophys.27.1.1.

2. Changeux J-P, Edelstein SJ (2005) Allosteric mechanisms of signal transduction. *Science* 308(5727):1424–1428.

3. Cui Q, Karplus M (2008) Allostery and cooperativity revisited. *Protein Sci Publ Protein Soc* 17(8):1295–1307.

4. Laskowski RA, Gerick F, Thornton JM (2009) The structural basis of allosteric regulation in proteins. *FEBS Lett* 583(11):1692–1698.

5. Hilser VJ, Wrabl JO, Motlagh HN (2012) Structural and energetic basis of allostery. *Annu Rev Biophys* 41. doi:10.1146/annurev-biophys-050511-102319.

6. Tsai C-J, Nussinov R (2014) A Unified View of "How Allostery Works." *PLoS Comput Biol* 10(2):e1003394.

7. CHANGEUX JP (1961) The feedback control mechanisms of biosynthetic L-threonine deaminase by. *Cold Spring Harb Symp Quant Biol* 26:313–318.

8. MONOD J, CHANGEUX JP, JACOB F (1963) Allosteric proteins and cellular control systems. *J Mol Biol* 6:306–329.

9. Monod J (1972) *Chance and Necessity an Essay on the Natural Philosophy of Modern Biology* (Monograph Collection (Matt - Pseudo)).

10. Fenton AW (2008) Allostery: an illustrated definition for the "second secret of life". *Trends Biochem Sci* 33(9):420–425.

11. Nussinov R, Tsai C-J, Ma B (2013) The underappreciated role of allostery in the cellular network. *Annu Rev Biophys* 42:169–189.

12. MONOD J, WYMAN J, CHANGEUX JP (1965) ON THE NATURE OF ALLOSTERIC TRANSITIONS: A PLAUSIBLE MODEL. *J Mol Biol* 12.

13. Koshland DEJ, Nemethy G, Filmer D (1966) Comparison of experimental binding data and theoretical models in proteins containing subunits. *Biochemistry (Mosc)* 5(1):365–385.

14. PERUTZ MF, MUIRHEAD H, COX JM, GOAMAN LCG (1968) Three-dimensional Fourier Synthesis of Horse Oxyhaemoglobin at 2.8 [angst] Resolution: The Atomic Model. *Nature* 219(5150):131–139.

15. Bolton W, Perutz MF (1970) Three dimensional fourier synthesis of horse deoxyhaemoglobin at 2.8 Angstrom units resolution. *Nature* 228(5271):551–552.

16. Garman E (00:00:00.0) Developments in x-ray crystallographic structure determination of biological macromolecules. *Sci N Y* 343(6175). doi:10.1126/science.1247829.

17. Koch MH, Vachette P, Svergun DI (2003) Small-angle scattering: a view on the properties, structures and structural changes of biological macromolecules in solution. *Q Rev Biophys* 36(2):147–227.

18. Rambo RP, Tainer JA (2013) Super-resolution in solution X-ray scattering and its applications to structural systems biology. *Annu Rev Biophys* 42:415–441.

19. Zhao J, Benlekbir S, Rubinstein JL (2015) Electron cryomicroscopy observation of rotational states in a eukaryotic V-ATPase. *Nature* 521(7551):241–245.

20. Cheng Y (2015) Single-Particle Cryo-EM at Crystallographic Resolution. *Cell* 161(3):450–457.

21. Popovych N, Sun S, Ebright RH, Kalodimos CG (2006) Dynamically driven protein allostery. *Nat Struct Mol Biol* 13(9):831–838.

22. Manglik A, et al. (2015) Structural Insights into the Dynamic Process of beta2-Adrenergic Receptor Signaling. *Cell* 161(5):1101–1111.

23. Hwang L, Hohlbein J, Holden S, Kapanidis A (2009) Single-Molecule FRET: Methods and Biological Applications. *Handbook of Single-Molecule Biophysics*, eds Hinterdorfer P, Oijen A (Springer US), pp 129–163.

24. Sustarsic M, Kapanidis AN (2015) Taking the ruler to the jungle: single-molecule FRET for understanding biomolecular structure and dynamics in live cells. *Curr Opin Struct Biol* 34:52–59.

25. Borbat P, Freed J (2013) Pulse Dipolar Electron Spin Resonance: Distance Measurements. *Structural Information from Spin-Labels and Intrinsic Paramagnetic Centres in the Biosciences*, Structure and Bonding., eds Timmel CR, Harmer JR (Springer Berlin Heidelberg), pp 1–82.

26. Jeschke G (2012) DEER distance measurements on proteins. *Annu Rev Phys Chem* 63:419–446.

27. Samanta D, Borbat PP, Dzikovski B, Freed JH, Crane BR (2015) Bacterial chemoreceptor dynamics correlate with activity state and are coupled over long distances. *Proc Natl Acad Sci U S A* 112(8):2455–2460.

28. Muirhead H, Greer J (1970) Three-dimensional Fourier synthesis of human deoxyhaemoglobin at 3.5 Angstrom units. *Nature* 228(5271):516–519.

29. Perutz MF (1970) Stereochemistry of cooperative effects in haemoglobin. *Nature* 228(5273):726–739.

30. Kantrowitz ER, Pastra-Landis SC, Lipscomb WN (1980) E. coli aspartate transcarbamylase: Part II: Structure and allosteric interactions. *Trends Biochem Sci* 5(6):150–153.

31. Allewell NM (1989) Escherichia coli Aspartate Transcarbamoylase: Structure, Energetics, and Catalytic and Regulatory Mechanisms. *Annu Rev Biophys Biophys Chem* 18(1):71–92.

32. Lipscomb WN, Kantrowitz ER (2012) Structure and Mechanisms of Escherichia coli Aspartate Transcarbamoylase. *Acc Chem Res* 45(3):444–453.

33. Volz K, Matsumura P (1991) Crystal structure of Escherichia coli CheY refined at 1.7-A resolution. *J Biol Chem* 266(23):15511–15519.

34. Cho HS, et al. (2000) NMR structure of activated CheY. *J Mol Biol* 297(3):543–551.

35. Lee S-Y, et al. (2001) Crystal Structure of Activated CheY: COMPARISON WITH OTHER ACTIVATED RECEIVER DOMAINS. *J Biol Chem* 276(19):16425–16431.

36. Simonovic M, Volz K (2001) A distinct meta-active conformation in the 1.1-A resolution structure of wild-type ApoCheY. *J Biol Chem* 276(31):28637–28640.

37. Formaneck MS, Ma L, Cui Q (2006) Reconciling the “old” and “new” views of protein allostery: a molecular simulation study of chemotaxis Y protein (CheY). *Proteins* 63(4):846–867.

38. Ma L, Cui Q (2007) Activation mechanism of a signaling protein at atomic resolution from advanced computations. *J Am Chem Soc* 129(33):10261–10268.

39. Wadhams GH, Armitage JP (2004) Making sense of it all: bacterial chemotaxis. *Nat Rev Mol Cell Biol* 5(12):1024–1037.

40. Hazelbauer GL, Falke JJ, Parkinson JS (2008) Bacterial chemoreceptors: high-performance signaling in networked arrays. *Trends Biochem Sci* 33(1):9–19.

41. Young MW, Kay SA (2001) Time zones: a comparative genetics of circadian clocks. *Nat Rev Genet* 2(9):702–715.

42. Dunlap JC, Loros JJ (2004) The neurospora circadian system. *J Biol Rhythms* 19(5):414–424.

43. Heintzen C, Liu Y (2007) The Neurospora crassa circadian clock. *Adv Genet* 58. doi:10.1016/S0065-2660(06)58002-2.

44. Baker CL, Loros JJ, Dunlap JC (2012) The circadian clock of Neurospora crassa. *FEMS Microbiol Rev* 36(1). doi:10.1111/j.1574-6976.2011.00288.x.

45. Zoltowski BD, et al. (2007) Conformational switching in the fungal light sensor Vivid. *Science* 316(5827):1054–1057.

46. Vaidya AT, Chen C-H, Dunlap JC, Loros JJ, Crane BR (2011) Structure of a light-activated LOV protein dimer that regulates transcription. *Sci Signal* 4(184). doi:10.1126/scisignal.2001945.

47. Conrad KS, Manahan CC, Crane BR (2014) Photochemistry of flavoprotein light sensors. *Nat Chem Biol* 10(10):801–809.

48. Frauenfelder H, Sligar SG, Wolynes PG (1991) The energy landscapes and motions of proteins. *Science* 254(5038):1598–1603.

49. Rasmussen BF, Stock AM, Ringe D, Petsko GA (1992) Crystalline ribonuclease A loses function below the dynamical transition at 220 K. *Nature* 357(6377):423–424.

50. Daniel RM, et al. (1998) Enzyme activity below the dynamical transition at 220 K. *Biophys J* 75(5):2504–2507.

51. Henzler-Wildman K, Kern D (2007) Dynamic personalities of proteins. *Nature* 450(7172):964–972.

52. Cooper A, Dryden DT (1984) Allostery without conformational change. A plausible model. *Eur Biophys J EBJ* 11(2):103–109.

53. Radley TL, Markowska AI, Bettinger BT, Ha J-H, Loh SN (2003) Allosteric Switching by Mutually Exclusive Folding of Protein Domains. *J Mol Biol* 332(3):529–536.

54. Ha J-H, Butler JS, Mitrea DM, Loh SN (2006) Modular enzyme design: regulation by mutually exclusive protein folding. *J Mol Biol* 357(4):1058–1062.

55. Tews I, et al. (2005) The structure of a pH-sensing mycobacterial adenylyl cyclase holoenzyme. *Science* 308(5724):1020–1023.

56. Schultz JE, Natarajan J (2013) Regulated unfolding: a basic principle of intraprotein signaling in modular proteins. *Trends Biochem Sci* 38(11):538–545.

57. Takala H, et al. (2014) Signal amplification and transduction in phytochrome photosensors. *Nature* 509(7499):245–248.

58. Tzeng S-R, Kalodimos CG (2011) Protein dynamics and allostery: an NMR view. *Curr Opin Struct Biol* 21(1):62–67.

59. Chervitz SA, Falke JJ (1996) Molecular mechanism of transmembrane signaling by the aspartate receptor: a model. *Proc Natl Acad Sci* 93(6):2545–2550.

60. Ottemann KM, Xiao W, Shin Y-K, Koshland DE (1999) A Piston Model for Transmembrane Signaling of the Aspartate Receptor. *Science* 285(5434):1751–1754.

61. Murphy OJ, Kovacs FA, Sicard EL, Thompson LK (2001) Site-Directed Solid-State NMR Measurement of a Ligand-Induced Conformational Change in the Serine Bacterial Chemoreceptor. *Biochemistry (Mosc)* 40(5):1358–1366.

62. Zhou Q, Ames P, Parkinson JS (2009) Mutational analyses of HAMP helices suggest a dynamic bundle model of input-output signalling in chemoreceptors. *Mol Microbiol* 73(5):801–814.

63. Zhou Q, Ames P, Parkinson JS (2011) Biphasic control logic of HAMP domain signalling in the Escherichia coli serine chemoreceptor. *Mol Microbiol* 80(3):596–611.

64. Airola MV, et al. (2013) HAMP Domain Conformers That Propagate Opposite Signals in Bacterial Chemoreceptors. *PLoS Biol* 11(2):e1001479.

65. Swain KE, Gonzalez MA, Falke JJ (2009) Engineered Socket Study of Signaling through a Four-Helix Bundle: Evidence for a Yin−Yang Mechanism in the Kinase Control Module of the Aspartate Receptor. *Biochemistry (Mosc)* 48(39):9266–9277.

66. Koshy SS, Li X, Eyles SJ, Weis RM, Thompson LK (2014) Hydrogen Exchange Differences between Chemoreceptor Signaling Complexes Localize to Functionally Important Subdomains. *Biochemistry (Mosc)* 53(49):7755–7764.

67. Nygaard R, et al. (2013) The dynamic process of beta(2)-adrenergic receptor activation. *Cell* 152(3):532–542.

Appendix A

A Plausible Model Describing Modulation of Bacterial Chemotaxis Kinase Activity by Alternation of Chemoreceptor Dynamics

Chapter two of this dissertation describes dynamics change in the protein interaction region (PIR) of bacterial chemoreceptors in response to ligand binding in the periplasmic domain. A plausible mechanical model has been envisaged to translate the dynamical change in PIR into modulation of kinase activity (Fig. Appendix A-1). The figure depicts a simplified picture of the association of bacterial chemoreceptor, the adaptor protein CheW and the kinase CheA along with the five domains of the dimeric kinase (P1 through P5). The regulatory P5 domain interacts with CheW and the PIR of receptor; the catalytic P4 domain binds ATP and phosphorylates the conserved histidine residue on P1 domain (H48 in *E. coli*); P3 is the dimerization domain; the least conserved P2 domain holds the response regulators CheY and CheB in order to facilitate phosphotransfer from the phosphorylated histidine in P1; and the P1 domain contains the conserved histidine residue. The P1 domain periodically interacts with P4 to receive phosphate and with the response regulators bound at the P2 domain to donate phosphate. This periodic motion is depicted in the figure with double-headed arrows. In the ligand-free state, the PIRs of the receptors are more reigid, and the periodic motion of P1 leads to efficient flow of the phosphate. However, upon ligand binding the PIR becomes comparatively more dynamic and the fluctuation of PIR backbone imposes additional dynamical modes on the P1 domain preventing the fruitful interaction of the P1 histidine with γ-phosphate of ATP bound at P4 domain and/or the correct interaction of the phosphorylated histidine with the response regulator aspartate. Interference in these two interactions renders CheA inactive and ultimately leads to cellular smooth swimming.

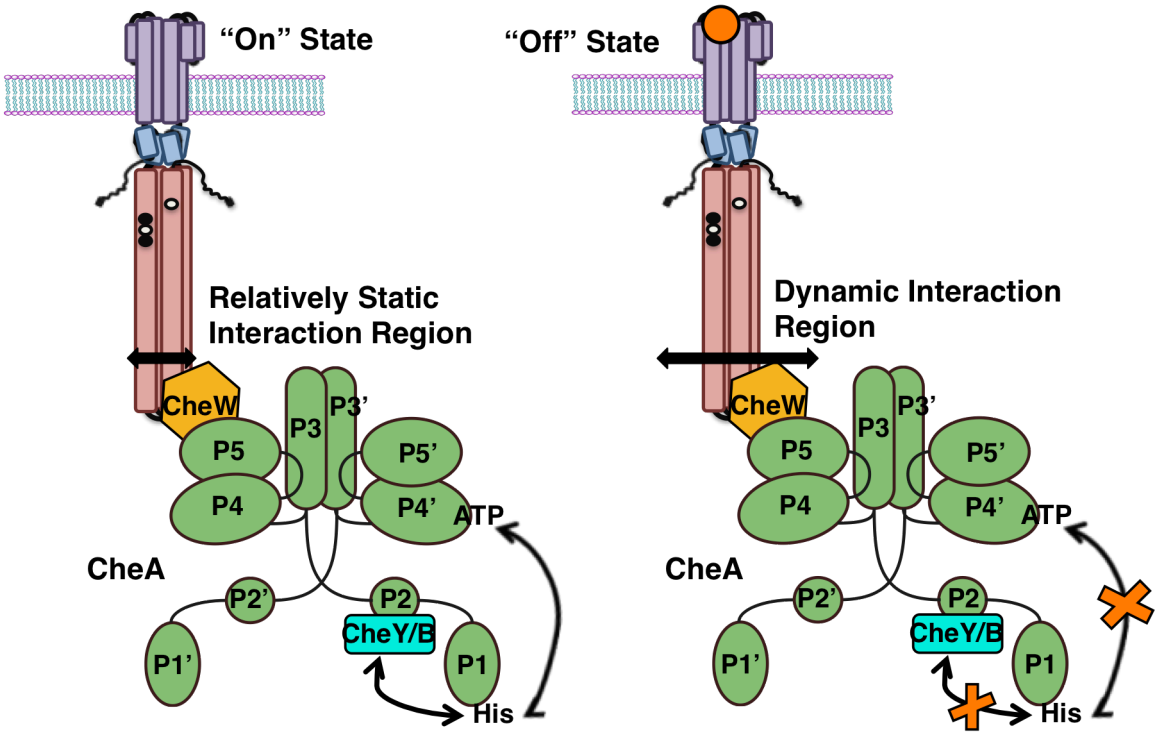

Figure Appendix A-1: A model that links dynamics in chemoreceptors with the kinase activity. A plausible mechanical model describes kinase activity regulation based on dynamics in the PIR of the bacterial chemoreceptors. Domains from different subunits of CheA are distinguished by apostrophe.

Appendix B

Redox State of Flavin Adenine Dinucleotide Cofactor Enables Aer-Mediated Bacterial Phototaxis in Response to Blue Light

Bacteria demonstrate physiological responses towards blue light exposure. Upon small duration exposure to blue light, *Salmonella typhimurium* and *Escherichia coli* tumble and removal of the light resumes smooth swimming of the cells. However, when exposed at intense light for long time, bacteria first tumble, then swim smoothly with lower speed before become paralyzed (1–3). In vivo gene knockout experiments verified the involvement of Aer (Chapter three) in this response (3). To formulate a mechanism of Aer regulation of bacterial responses to blue light, we tested the effect of blue light on the redox state of FAD in Aer. Light of 445 nm reduces fully oxidized FAD in Aer solubilized in 0.1 % DDM to the anionic semiquinone (ASQ) state, however the reduction process is expedited in presence of 13.3 mM DTT and/or 31 mM EDTA pH 8.0 (Fig. Appendix B-1A). We also have observed this reduction when Aer is incorporated into nanodisc assembled from *E. coli* polar lipid and the membrane scaffold protein MSP1E3D1 (Fig. Appendix B-1B). Chapter three describes that ASQ state deactivates the chemotaxis kinase protein CheA, and thus photoreduction of FAD to ASQ state would cause cellular smooth swimming and fail to explain tumbling response to blue light. Further explorations are required to reconcile this discrepancy. Involvement of other proteins should also be considered.

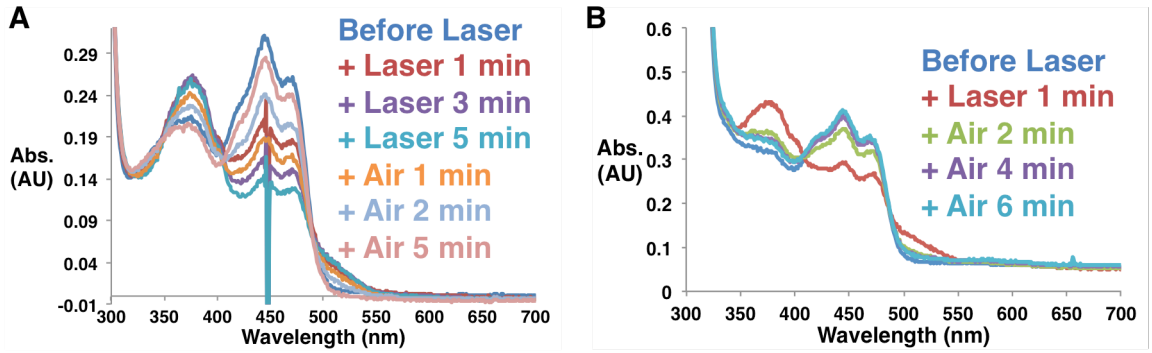

Figure Appendix B-1: Blue light reduction of FAD cofactor in EcAer. Blue light (445 nm) reduction and aerial reoxidation of FAD in Aer solubilized in 0.1 % DDM, and in presence of 13.3 mM DTT and 31 mM EDTA pH 8.0 (A) or in Aer incorporated into nanodisc (B). The negative spike in (A) around 450 nm is due to scattering of the laser light itself.

References:

1. Taylor BL, Koshland DE (1975) Intrinsic and extrinsic light responses of Salmonella typhimurium and Escherichia coli. *J Bacteriol* 123(2):557–569.

2. Taylor BL, Miller JB, Warrick HM, Koshland DEJ (1979) Electron acceptor taxis and blue light effect on bacterial chemotaxis. *J Bacteriol* 140(2):567–573.

3. Wright S, Walia B, Parkinson JS, Khan S (2006) Differential activation of Escherichia coli chemoreceptors by blue-light stimuli. *J Bacteriol* 188(11):3962–3971.